Co-electro-polymerization/generation of poly-terthiophene/Au nanoparticle incorporated thin-film at a micro liquid|liquid interface

A Dissertation Presented

By

Siamak Khoshrou

Submitted to the Graduate School of the

Memorial University of Newfoundland in partial fulfillment

of the requirements for the degree of

MASTER OF SCIENCE

in

Chemistry

2021

Declaration of Committee

Name: **Siamak Khoshrou**

Degree: **Master of Chemistry**

Title: **Co-electro-polymerization/generation of poly-terthiophene/Au nanoparticle incorporated thin-film at a micro liquid/liquid interface**

Committee:

Chair: **Sunil V. Pansare**
Department Head

Jane Stockmann
Supervisor

Peter G. Pickup
Committee Member

Chris Rowley
Committee Member

Abstract

Electroactive thin films are desirable for a wide array of applications, including catalysis, energy conversion, and (bio)sensor technologies. Herein, a novel strategy has been developed for the simultaneous electrochemical formation of polythiophene (PT) films with gold (Au) nanoparticle (NP) generation. In this method, $AuCl_4^-$ (aq) is reduced at a water|1,2-dichloroethane (w|DCE) micro liquid|liquid interface by terthiophene (TT) positioned in the organic phase. The liquid|liquid interface is advantageous as it is molecularly sharp/smooth and highly reproducible, which distinguishes it from solid/solution interfaces where surface morphology can play a critical role. To further enhance the sensitivity of this technique, a micro interface between two immiscible electrolyte solutions (ITIES) was employed by use of a micropipette (25 μm in diameter). The morphology and size of the Au NPs at the ITIES was investigated by changing the applied potential, aqueous phase pH, and $[KAuCl_4]$:[TT] concentration ratio. Three different ratios, 1:1, 1:2 and 1:3, where chosen and paired with three pH regimes: 2, 5.5 and 8.5. The as-prepared Au-NP/PT films were then analyzed by Transmission electron microscopy (TEM) and Scanning electron microscopy (SEM), while electrodeposition was monitored by cyclic voltammetry. Interestingly, Au NP size increased concomitantly with pH and the ratio of $[KAuCl_4]$:[TT]. Bithiophene was also investigated; however, no film formation was observed.

Preliminary results using 4,5-didecoxy-1,8-bis(dithiafulvenyl)pyrene ($C_{10}C_{10}$bisDTF) are also discussed with respect to its electro-polymerization/deposition on to a carbon fiber ultramicroelectrode (UME) followed by electrodeposition of Au nanoparticles via electrode reduction of $KAuCl_4$(aq). These modified electrodes have been evaluated as selective dopamine (DA) sensors versus ascorbic acid.

Acknowledgements

I appreciate having had the opportunity to interact with many intelligent scientists, and support staff over the past two years at Memorial University of Newfoundland. I would first like to thank my supervisor, Professor Jane Stockmann, for her abiding support and guidance during my graduate studies. Dr. Stockmann always brought her powerful intellect to bear on any research questions that I brought to her and gave selflessly of her time. I do not have enough words to express my appreciation but without her constant encouragement, insightful advice and patient instruction, the accomplishment of my dissertation would not been possible. I would also like to extend my gratitude to the committee members, Professor Peter G. Pickup and Professor Chris Rowley, for their valuable contributions on my research projects. I would also like to acknowledge Professor Sunil V. Pansare, Department Head, for providing helpful comments and advice. Many of the faculty and staff have also provided support and encouragement over the years, especially Professor Christina Bottaro, Professor Erika Merschrod, Professor Céline Schneider, and Debbie Hickey.

I am grateful to my lab mates, who were not only people I worked with, but also my friends. I would like to thank Reza Moshrefi, Nazanin Ahmadinasab, Qi Jiang and Abhishek Suryawanshi, and all the others. I would like to thank Josh Walsh and Dr. Graham J. Bodwell group in the Chemistry department of Memorial University for providing $C_{10}C_{10}$BisDTF monomer.

Finally, I would like to thank my family, Mohammadali Khoshrou, Homeyra Azizi, Babak Khoshrou and Sadaf Khoshrou. Without them, I would not be the person I am today,

and I thank them from the bottom of my heart. Most of all, I thank my Spouse Niloofar Mahdavi, without whom my graduate student life would have been one-dimensional

List of Abbreviations

Abbreviation	Meaning
PT	Polythiophene
NP	Nanoparticle
W	Water
DCE	Dichloroethane
TT	Terthiophene
BT	Bithiophene
ITIES	Interface between Two Immiscible Electrolyte Solutions
TEM	Transmission electron microscopy
SEM	Scanning electron microscopy
UME	Ultra-Micro Electrode
Aq	Aqueous
Org	Organic
DA	Dopamine
NMR	Nuclear Magnetic Resonance
IT	Ion Transfer
ET	Electron Transfer
WE	Working Electrode
CE	Counter Electrode

CV	Cyclic voltammogram
PPW	Polarizable Potential Window
RE	Reference Electrode
NB	Nitrobenzene
THF	Tetrahydrofuran
DCM	Dichloromethane
IUPAC	International Union of Pure and Applied Chemistry
PA	Polyacetylene
PT	Polythiophene
PANI	Polyaniline
PPy	Polypyrrole
GCE	Glassy Carbon Electrode
TT	Terthiophene
CVD	Chemical Vapor Deposition
CT	Charge Transfer
IL	Ionic Liquid
SHE	Standard Hydrogen Electrode

EDX	Energy Dispersive X-Ray Analysis
ITO	Indium Tin Oxide
HPLC	High-Performance Liquid Chromatography
UV-vis	Ultraviolet–visible spectroscopy

Table of Contents

List of Figures

List of Appendix Figures

Chapter 1. Introduction

1.1. Surface modification

In general, surface modification refers to any physical, chemical, or biological change on the surface of a material and it usually results in a solid layer. Surface modification aims to change properties such as roughness, surface charge, hydrophilicity, surface energy, or sample reactivity.[1-3] Surface modification can favorably impact on detection of different analytes like metal ions, anions, or organic species. Some of the techniques for modifying electrode surfaces are covalent bonding, chemisorption, and electrodeposition.[4-6] One prevalent surface modification method is electrodeposition, which usually occurs at the interface of two phases and is based on charge transfer. In this method, the driving force is the electric potential to make a deposited coating layer and usually the charge transfer reaction is exploited to result in a metal or polymer nanostructured layer.[7, 8]

1.2. Electrochemical sensors

A sensor is a device that responds to a physical or chemical signal and converts it into recordable data often as an electrical current. Some of the most critical factors in a sensor are selectivity, sensitivity, and stability.[9] There is a wide range of sensors and among them, electrochemical sensors, because of unique properties, attract a great deal of interest. New types of electrochemical sensors have been generated based on ion transfer (IT) and electron transfer (ET) across the liquid|liquid interface and deposition of the nanoparticles

by applying a potential. Because of some features of nanomaterials, like high surface area, interest in developing nanoparticles in electrochemical sensors has increased in the past decades.[10]

Common materials for developing electrochemical electrodes are carbon, gold, and platinum. From an economic point of view, as some metals like palladium, gold, platinum, and silver are expensive, researchers are trying to fabricate more cost-effective electrodes by two strategies: 1) using cheaper metals like iron, aluminum and zinc, and their composites with other materials like carbon nanotubes and graphene; 2) coating a very thin layer of expensive metals onto cheaper metals. In general, nanomaterials like metal nanoparticles, metal oxide nanoparticles, and carbon nanomaterials are among the most popular electrode surface modifiers due to the their high electrical conductivity, large surface area, and superior catalytic properties.[11-13]

1.3. Electrochemical surface modification

In electrochemical surface modification (electrodeposition), the potential of the electrode is changed by applying an external electric field, leading to a reduction or oxidation reaction at the electrode surface. As the electrochemical reactions occur at the interface between the solution and electrode, the surface nature and properties of the electrode play crucial roles in its performance.[14] Many efforts have been made to enhance the electrode electroactivity and interfacial charge transfer by decorating the electrode surface with functional groups.[15,16] Some nanomaterials that have been successfully

fabricated through electrodeposition are gold nanoparticles,[17] silver nanoparticles,[18] nickel nanoparticles,[19] polyaniline nanorods,[20] polypyrrole nanowires,[21] and pyrene nanosheets.[22]

Some advantages of electrochemical surface modification are enhanced thermal stability, short deposition time, controlling the diffusion process, as well as excellent reproducibility and stability.[12, 23, 24] The most powerful electrochemical instrument to study redox processes and electrodeposit the nanostructures is a potentiostat, an analytical instrument designed to control the working electrode's potential in an electrochemical cell. The potentiostat measures the current flow between the working electrode (WE) and counter electrode (CE) and records the current-potential response according to a pulse sequence, *e.g.*, a cyclic voltammogram (CV). Usually a CV contains three sections, forward scanning to positive potentials, then scanning in the opposite direction toward negative potential and finally back to the initial potential. CVs reveal redox peaks in the *i-V* curve, and a multi-ET process can present several redox couple peaks, based on the number of charges transferred.

1.4. History of liquid|liquid interfaces

Verwey and Niessen[25] were the first persons who introduced the double layer at the interface between two immiscible electrolyte solutions (ITIES). They considered the two sides of the interface as independent phases, placed back-to-back at the interface, one phase contains excess negative charge, and the other has an equal excess of positive charge. Later this model was improved by Gavach *et al.*,[26] in the 1960s. He discovered that by applying a potential across the liquid|liquid interface, the interface can be polarized. The liquid|liquid

interface is polarizable since the dissolution of hydrophilic and hydrophobic supporting electrolyte salts in aqueous and organic phases, respectively, results in little to no ion transfer over a typically 1 V potential range, called the polarizable potential window (PPW). The IT potentials of salts present in the phase determine the size of the PPW.

A four-electrode potentiostat was introduced by Samec[27] in 1977 for the first time and his pioneering work has changed the electrochemical investigation of various interactions at the ITIES into the modern field of electrochemistry. In the four-electrode electrochemical cell, one CE and one reference electrode (RE) were placed in both the aqueous and organic phases. By applying an external potential to the REs, RE_{aq} and RE_{org}, the interface between the hydrophilic aqueous and hydrophobic organic phases, was polarized and the induced current across the ITIES was measured by the two counter electrodes CE_{aq} and CE_{org}.[27] Since Taylor *et al*.[28] studied the IT at the liquid|liquid interface using a micropipette in 1986, micro and nanopipette electrochemically studying have attracted more attention.[29]

1.5. Liquid|liquid interfacial electrochemistry

1.5.1. Organic phase in liquid|liquid interface

To have an ITIES, two liquids should be ideally immiscible with each other; one of the phases is usually water and the other is an immiscible polar organic solvent. Another critical feature of the organic solvent in a liquid|liquid electrochemical cell is having a wide PPW to provide the opportunity to study ET and IT in a broad potential range. Two of the most popular organic solvents for electrochemical purposes are 1,2-dichloroethane

(DCE),[30] and nitrobenzene (NB),[31] while, some other organic solvents are tetrahydrofuran (THF),[32] dichloromethane (DCM),[33] and toluene.[34]

1.5.2. Galvani Potential Difference

One very important term to study electrochemical phenomenon is the Galvani potential difference. According to International Union of Pure and Applied Chemistry (IUPAC), the Galvani potential or Galvani potential difference is the electric potential difference between the bulk of two phases.[35] In other words, Galvani potential difference is the potential drop across the interface between two phases. To determine the Galvani potential difference, two immiscible phases should be in equilibrium, and it is calculated based on the electrochemical potential of each phase. Because of differences in physical properties of solvents, such as hydrophobicity, species dispersed in aqueous and organic phases have different chemical potentials, resulting in a different Galvani potential at the ITIES.[36]

1.5.3. Nernst equation

The Nernst equation expresses the potential of an electrochemical cell for a reversible system at equilibrium. According to the Nernst equation, the potential difference at an ITIES can be shown by the following equation (Eq. 1.1):

$$\Delta_{\mathrm{o}}^{\mathrm{w}}\phi = \Delta_{\mathrm{o}}^{\mathrm{w}}\phi_i^0 + \frac{RT}{n_i F}\ln\left(\frac{a_{\mathrm{o}}^i}{a_{\mathrm{w}}^i}\right) = \Delta_{\mathrm{o}}^{\mathrm{w}}\phi_i^0 + \frac{RT}{n_i F}\ln\left(\frac{\gamma_o^i}{\gamma_w^i}\right) + \frac{RT}{n_i F}\ln\left(\frac{C_o^i}{C_w^i}\right) = \Delta_{\mathrm{o}}^{\mathrm{w}}\phi_i^{0\prime} + \frac{RT}{n_i F}\ln\left(\frac{C_o^i}{C_w^i}\right) \quad (1.1)$$

Where a_o^i, γ_o^i and c_o^i refer to the activity, activity coefficient, and concentration of species *i*, *w*, and *o* show the aqueous and organic phase, respectively. n_i, F, R, and T represent the charge number of species *i*, Faraday's constant, the universal gas constant, and temperature in Kelvin, respectively. For the simplicity $\Delta_o^w \phi_i^{0'}$ is assumed based on the following equation (Eq. 1.2):

$$\Delta_o^w \phi = \Delta_o^w \phi_i^0 + \frac{RT}{n_i F} \ln\left(\frac{C_o^i}{C_w^i}\right) \quad (1.2)$$

where c_α^i is the concentration of species *i* in phase α and $\Delta_o^w \phi_i^0$ is its standard ion transfer potential as defined by the equation (Eq. 1.3):

$$\Delta_o^w \phi_i^{0,w\to o} = \frac{\Delta G_{tr,i}^0}{n_i F} = \frac{\mu_i^{0,o} - \mu_i^{0,w}}{n_i F} \quad (1.3)$$

Where the $\mu_i^{0,o}$ and $\mu_i^{0,w}$ are the standard chemical potentials of species *i* in the organic and aqueous phases, respectively, and $\Delta G_{tr,i}^0$ is the standard Gibbs free energy of IT of species *i* from aqueous to the organic phase.

1.5.4. Electrodeposition at liquid|liquid Interfaces

The ITIES offers a unique environment for synthesizing nano/micro-structured materials that are difficult or impossible to prepare by other methodologies. Electrochemical deposition is an intrinsic process and is done by redox reactions at the electrode surface or across the ITIES:

$$\boldsymbol{Ox_1 + e \rightarrow Red_1} \qquad \text{Electrode}$$

$$Red_1 + Ox_2 \rightarrow Ox_1 + Red_2 \qquad \text{ITIES}$$

Although much research has been done on electrodeposition of nanoparticles at ITIES, the understanding of the electrochemical deposition process at the ITIES has been hampered as the deposited nanoparticles have a tendency to aggregate.[37] By applying the potential across the interface, electrons are pushed or pulled across the ITIES to nucleate and grow nanoparticles or form a film at the interface (Figure 1.1).[38] A wide range of metal nanoparticles has been electrodeposited at the ITIES, including Au, Pd, Ag and Cu.[6, 39-41] Metal nanoparticle electrodeposition is done by reducing metal salt precursors dissolved in one phase (like $KAuCl_4$ in the aqueous phase) and using the electrons of a reducing agent present in another phase (like ferrocene in the organic phase).[6]

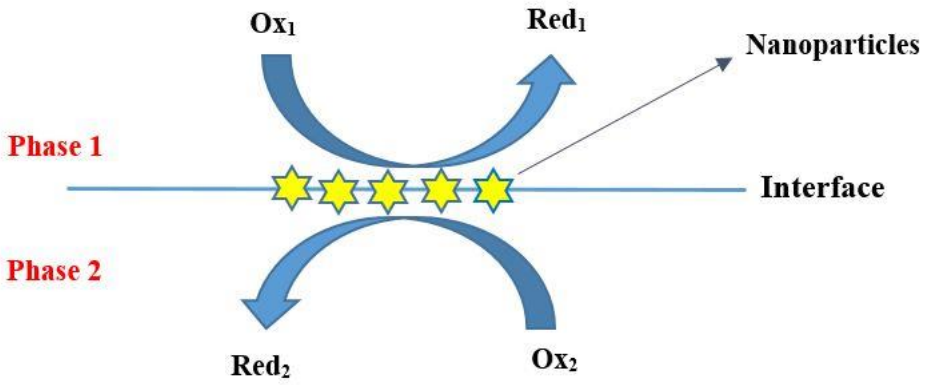

Figure 1.1 Formation of nanoparticles at the ITIES using simultaneous redox reactions

1.6. Electrochemical polymerization

Over the last decades, different methods like freeze/thaw,[42] solution blending,[43] solvent casting,[44] and electrochemical methods[45] have been used to deposit a film at the interface. However, among these different techniques, electrochemical polymerization or electro-polymerization has attracted the most attention.

Electro-polymerization is a straightforward way to generate a polymer film by applying an external potential to the working electrode with respect to a reference electrode. One very popular way for electro-polymerization is employing CV. By scanning for a couple of cycles, a multilayered thin film deposits on the electrode surface. Indeed, the film physical/chemical properties and performance can be easily tuned by changing experimental parameters such as monomer concentration, scan rate, potential range and the number of cycles.[46-48] A new way to synthesize conductive polymers is electro-polymerization at an ITIES in which the monomer and oxidizing agent should be present in the organic and aqueous phases, respectively, and the electro-polymerization is done by redox reactions.

1.6.1. Electrochemical polymerization of thiophene

Because of extraordinary electrical, magnetic, and optical properties, conductive polymers such as polyacetylene (PA), polypyrrole (PPy), polythiophene (PT), and polyaniline (PANI) have a wide range of electrochemical applications.[49] Among them polythiophene is a promising material in the electrocatalytic field of research due to its

properties like excellent operational stability, sensitivity, reproducibility and repeatability.[50, 51]

Polythiophene is polymerized thiophene, featuring chains of the planar five-membered rings. The common thiophene derivatives are bithiophene and terthiophene; one way to synthesize polythiophene is using these monomers in an electrochemical cell and applying potential suitable to induce their oxidation.[52, 53] Owing to their relatively low redox potentials, use of bithiophene or terthiophene reduces the required amount of applied potential to initiate electrochemical polymerization, which decreases the possibility of side reactions during the process, like mislinkages and overoxidation of the polymers.[52, 54] Moreover, in the use of these monomers, the number of nucleation sites and the rate of polymer nucleation on the electrode surface are considerably enhanced, leading to more homogeneous polymer films.[52]

1.7. Carbon-based electrodes

Carbon is one of the most ubiquitous elements on the earth and it is relatively inexpensive and available in a variety of forms. Carbon-based electrodes are among the most common electrodes in today's scientific world, and the best-known carbon electrodes include glassy carbon, carbon fiber, carbon paste, screen printed electrodes, graphite, fullerene, and carbon nanotubes. For instance, the reasons behind the great popularity of graphene-based electrode are its high electrocatalytic activity and biocompatibility.[55]

Among the carbon electrodes used to fabricate electrochemical sensors the glassy carbon electrode (GCE) is particularly important because of its unique properties. Besides remarkable mechanical and electrical properties and being chemically inert, some other GCE properties are high electrochemical sensitivity and stability, along with it being inexpensive and easy to prepare.[56] The main disadvantage of the carbon-based electrodes is their high overpotential, meaning that the potential needed for reduction or oxidation of a particular species is higher than the thermodynamically calculated potential. This is because of the lack of appropriate interaction between the carbon surface and species molecules in unmodified carbon electrodes.[57] To address this issue and enhance the electrochemical reactivity of the carbon-based electrodes, they are usually functionalized with organic or inorganic electroactive compounds.[58]

Electrochemical surface modification of GCE with metal nanoparticles like gold nanoparticles,[59] platinum nanoparticles,[60] and palladium nanoparticles[61] is done to enhance its electrochemical activity. Electro-polymerization at GCE surface is another way to modify the electrode by oxidation of monomers and deposition of a thin polymer film on the GCE surface.[62]

1.8. Electrochemical surface modification for dopamine detection

One important application of electrochemical surface modification is synthesizing electrodes to detect biological species like dopamine. Dopamine is an important

neurotransmitter that plays a vital role in the human nervous system and inappropriate performance of DA leads to diseases such as schizophrenia, alzheimer's and Parkinson.[63] Although the current methods to sense dopamine show relatively good performance, in situ dopamine detection is still challenging.

In this approach, different electrochemical and non-electrochemical methods have been used to increase the electrode's efficiency and the electrochemical sensors show high efficiency for dopamine detection. The issue with these electrodes is that some molecules like ascorbic acid and uric acid have similar redox potentials to dopamine and interfere in its detection.[64] Many efforts have been made to modify the electrode surface and enhance the electrocatalytic activity of the carbon surface towards dopamine detection. Some modifiers of the electrode surface are metal nanoparticle,[65] carbon materials,[66] polymeric materials,[67] and ionic liquids.[68] For example, Yang *et al*.[69] electrochemically modified the surface of a carbon aerogel electrode with PPy to detect dopamine. They electro-polymerized a uniform and compact molecularly imprinted polymer film on an electrode surface and chose PPy since it has high conductivity and biocompatibility.

1.9. Scope of Thesis

In this project, two different studies were carried out: 1) electro-polymerization of Au NPs/Poly-terthiophene thin-film at a micro liquid|liquid interface and 2) electrochemical detection of DA and ascorbic acid by using a modified ultramicroelectrode, surface modified with polymerized 4,5-didecoxy-1,8-bis(dithiafulvenyl)pyrene ($C_{10}C_{10}$bisDTF) and $KAuCl_4$.

The first study demonstrates an approach to form electrodeposited self-assembly of Au NPs at the ITIES and a thin-film. We also provide a better understanding of IT and ET mechanisms across the ITIES and use CV to polymerize TT at the ITIES. In this approach, $KAuCl_4$, as supporting electrolyte and eventual source of Au NPs in the aqueous phase, and TT, as electron donor and monomer in the organic phase, were brought into contact. So, an ET redox reaction happens from TT to $AuCl_4^-$ at the ITIES. As a result of this reaction, $AuCl_4^-$ is reduced to Au NPs and TT molecules are oxidized to the cation radical ($TT^{2+\cdot}$). Thin-film is formed across the ITIES by coupling of these $TT^{2+\cdot}$ radicals. The research is done in micro-sized ITIES to decrease the ohmic potential drop and sense weak currents. The film formation at ITIES, structure, and morphology of the Au NPs are examined by SEM and TEM. The experiments were conducted at three different pH values of the aqueous phase to investigate the effect of pH values on the morphology of electrodeposited Au NPs and thin-film properties.

In the second study, DA and ascorbic acid electrochemical detection was carried out using a modified UME. The UME surface modification is done by film electrogeneration with $C_{10}C_{10}$BisDTF monomer and then electrodeposition of Au NPs. The effect of electrode surface modification on DA and ascorbic acid detection is studied using a CV instrument. The results show low sensitivity of unmodified UME regarding DA and ascorbic acid detection, however, surface modification enhances the DA and ascorbic acid detection. SEM is used to examine the film formation and electrodeposition of Au NPs on a solid|solution interface.

1.10. References:

(1) Mahtabani, A.; Rytöluoto, I.; Anyszka, R.; He, X.; Saarimäki, E.; Lahti, K.; Paajanen, M.; Dierkes, W.; Blume, A. *ACS Appl. Polym. Mater.* **2020**, *2*, 3148.

(2) Jallo, L. J.; Schoenitz, M.; Dreizin, E. L.; Dave, R. N.; Johnson, C. E. *Powder Technol* **2010**, *204*, 63.

(3) Zareidoost, A.; Yousefpour, M.; Ghaseme, B.; Amanzadeh, A. *J Mater Sci Mater Med* **2012**, *23*, 1479.

(4) Jana, M.; Khanra, P.; Murmu, N. C.; Samanta, P.; Lee, J. H.; Kuila, T. *Phys. Chem. Chem. Phys.* **2014**, *16*, 7618.

(5) Forget, A.; Limoges, B.; Balland, V. *Langmuir* **2015**, *31*, 1931.

(6) Moshrefi, R.; Suryawanshi, A.; Stockmann, T. J. *Electrochem Commun* **2021**, *122*, 106894.

(7) Gurrappa, I.; Binder, L. *Sci Technol Adv Mater* **2016**, *9*, 043001.

(8) Naseri, M.; Fotouhi, L.; Ehsani, A. *Chem. Rec.* **2018**, *18*, 599.

(9) Wang, Y.; Nie, Z.; Li, X.; Zhao, Y.; Wang, H. *Sens. Actuators B Chem.* **2021**, *346*, 130539.

(10) Bramhaiah, K.; Pandey, I.; Singh, V. N.; Kavitha, C.; John, N. S. *J Nanopart Res* **2018**, *20*.

(11) Scanlon, M. D.; Smirnov, E.; Stockmann, T. J.; Peljo, P. *Chem Rev* **2018**, *118*, 3722.

(12) Gao, F.; Du, L.; Zhang, Y.; Zhou, F.; Tang, D. *Biosens Bioelectron* **2016**, *86*, 185.

(13) George, J. M.; Antony, A.; Mathew, B. *Microchimica Acta* **2018**, *185*.

(14) Sandhyarani, N. *Electrochemical Biosensors*, ed. A. A. Ensafi (Elsevier, Amsterdam), **2019**, 45.

(15) Liu, T.; Zhang, Y.; Zhang, X.; Wang, L.; Zhao, S.-X.; Lin, Y.-H.; Shen, Y.; Luo, J.; Li, L.; Nan, C.-W. *J. Mater. Chem.* **2018**, *6*, 4649.

(16) Huang, Y.; Huang, Y.; Hu, X. *Electrochim. Acta* **2017**, *231*, 294.

(17) Zou, C. e.; Yang, B.; Bin, D.; Wang, J.; Li, S.; Yang, P.; Wang, C.; Shiraishi, Y.; Du, Y. *Colloid Interface Sci.* **2017**, *488*, 135.

(18) Pompilio, A.; Geminiani, C.; Bosco, D.; Rana, R.; Aceto, A.; Bucciarelli, T.; Scotti, L.; Di Bonaventura, G. *Front. microbiol* **2018**, *9*.

(19) Aldana-González, J.; Romero-Romo, M.; Robles-Peralta, J.; Morales-Gil, P.; Palacios-González, E.; Ramírez-Silva, M. T.; Mostany, J.; Palomar-Pardavé, M. *Electrochim. Acta* **2018**, *276*, 417.

(20) Kai Wang, J. H., Zhixiang Wei *J. Phys. Chem. C* **2010**, *114*, 8062.

(21) Huang, Z.-H.; Song, Y.; Xu, X.-X.; Liu, X.-X. *ACS Appl. Mater. Interfaces* **2015**, *7*, 25506.

(22) Lu, G.; Shi, G. *J. Electroanal. Chem.* **2006**, *586*, 154.

(23) Kyo-Han Kim, N. R. *Dent. Mater. J.* **2009**, *28*, 20.

(24) Park, Y.-U.; Bai, J.; Wang, L.; Yoon, G.; Zhang, W.; Kim, H.; Lee, S.; Kim, S.-W.; Looney, J. P.; Kang, K.; Wang, F. *J. Am. Chem. Soc.* **2017**, *139*, 12504.

(25) E. J. W. Verwey, K. F. N. *Philos. Mag. Lett. Series 7* **1939**, *28*, 435.

(26) C. Gavach, T. M., J. Guastalla, C. R. *Acad. Sci.* **1968**, *266*, 1196.

(27) Z. Samec, V. M., J. Koryta, M.W. Khalil *J. Electroanal. Chem.* **1977**, *83*, 393.

(28) G. taylor, H. h. j. g. *J. Electroanal. Chem.* **1986**, *208*, 179.

(29) Liu, S.; Li, Q.; Shao, Y. *Chem. Soc. Rev.* **2011**, *40*, 2236.

(30) Burgoyne, E. D.; Molina-Osorio, A. F.; Moshrefi, R.; Shanahan, R.; McGlacken, G. P.; Stockmann, T. J.; Scanlon, M. D. *Analyst* **2020**, *145*, 7000.

(31) Shul, G.; Opallo, M.; Marken, F. *Electrochim. Acta* **2005**, *50*, 2315.

(32) Aydin, F.; Yilmaz, E.; Soylak, M. *Food Chem.* **2018**, *243*, 442.

(33) Zhu, Z.; Zhang, Y.; Wang, J.; Li, X.; Wang, W.; Huang, Z. *J. Chromatogr. A* **2019**, *1601*, 104.

(34) Chen, R.; Ata, M. S.; Zhao, X.; Clifford, A.; Puri, I.; Zhitomirsky, I. *Colloid Interface Sci.* **2017**, *499*, 1.

(35) Deng, H.; Dick, J. E.; Kummer, S.; Kragl, U.; Strauss, S. H.; Bard, A. J. *Anal. Chem.* **2016**, *88*, 7754.

(36) *IUPAC, Gold book*, Version 2.3.1 **2012**.

(37) Stockmann, T. J.; Ding, Z. *J. Electroanal. Chem.* **2010**, *649*, 23.

(38) Johans, C.; Liljeroth, P.; Kontturi, K. *Phys. Chem. Chem. Phys.* **2002**, *4*, 1067.

(39) Inagaki, C. S.; Oliveira, M. M.; Zarbin, A. J. G. *J Colloid Interface Sci* **2018**, *516*, 498.

(40) Booth, S. G.; Chang, S.-Y.; Uehara, A.; La Fontaine, C.; Cibin, G.; Schroeder, S. L. M.; Dryfe, R. A. W. *Electrochim. Acta* **2017**, *235*, 251.

(41) Fei Li, M. E., Jidong Guo, Patrick R. Unwin *J. Phys. Chem. C* **2009**, *113*, 3553.

(42) Aslan, E.; Patir, I. H.; Ersoz, M. *Chem. - A Eur. J.* **2015**, *21*, 4585.

(43) Qi, X.; Hu, X.; Wei, W.; Yu, H.; Li, J.; Zhang, J.; Dong, W. *Carbohydr. Polym* **2015**, *118*, 60.

(44) Zeng, X.; Yang, J.; Yuan, W. *Eur. Pol. J.* **2012**, *48*, 1674.

(45) Wang, L.-F.; Rhim, J.-W.; Hong, S.-I. *LWT - Food Sci. Technol.* **2016**, *68*, 454.

(46) Fonseca, S. M.; Moreira, T.; Parola, A. J.; Pinheiro, C.; Laia, C. A. T. *Sol. Energy Mater. Sol. Cells* **2017**, *159*, 94.

(47) Achour, A.; Soussou, M. A.; Ait Aissa, K.; Islam, M.; Barreau, N.; Faulques, E.; Le Brizoual, L.; Djouadi, M. A.; Boujtita, M. *Thin Solid Films* **2014**, *571*, 168.

(48) Ramachandran, A.; Panda, S.; Karunakaran Yesodha, S. *Sens. Actuators B Chem.* **2018**, *256*, 488.

(49) Liu, Y.; Liu, J.; Liu, J.; Gan, W.; Ye, B.-c.; Li, Y. *Microchimica Acta* **2017**, *184*, 1285.

(50) Poddar, A. K.; Patel, S. S.; Patel, H. D. *Polym Adv Technol* **2021**.

(51) Faisal, M.; Harraz, F. A.; Al-Salami, A. E.; Al-Sayari, S. A.; Al-Hajry, A.; Al-Assiri, M. S. *Mater. Chem. Phys.* **2018**, *214*, 126.

(52) Harraz, F. A.; Faisal, M.; Jalalah, M.; Almadiy, A. A.; Al-Sayari, S. A.; Al-Assiri, M. S. *Appl. Surf. Sci.* **2020**, *508*, 145226.

(53) Yen Wei, C.-C. C., Jing Tian, Guang-Way Jang, Kesyin F. Hsueh *Chem. Mater.* **1991**, *3*, 888.

(54) Leon, A. C.; Imperial, R. E. S.; Chen, Q.; Advincula, R. C. *Macromol Mater Eng* **2019**, *304*, 1800722.

(55) B. Krische, m. Z. *Synth. Met* **1989**, *28*, 263.

(56) Ming Zhou, Y. Z., Shaojun Dong *Anal. Chem.* **2009**, *81*, 5603.

(57) Ying Li, S.-M. C. *Int. J. Electrochem. Sci.* **2012**, *7*, 2175

(58) Blandón-Naranjo, L.; Hoyos-Arbeláez, J.; Vázquez, M. V.; Della Pelle, F.; Compagnone, D. *J. Sens.* **2018**, *2018*, 1.

(59) Qiu, L.; Zou, H.; Wang, X.; Feng, Y.; Zhang, X.; Zhao, J.; Zhang, X.; Li, Q. *Carbon* **2019**, *141*, 497.

(60) Li, T.; Xu, J.; Zhao, L.; Shen, S.; Yuan, M.; Liu, W.; Tu, Q.; Yu, R.; Wang, J. *Talanta* **2016**, *159*, 356.

(61) Koçak, S. *Electroanalysis* **2020**, *33*, 375.

(62) Koçak, Ç. C.; Koçak, S. *Electroanalysis* **2019**, *32*, 358.

(63) Abdel-Aziz, A. M.; Hassan, H. H.; Badr, I. H. A. *Anal. Chem.* **2020**, *92*, 7947.

(64) Banerjee, S.; McCracken, S.; Hossain, M. F.; Slaughter, G. *Biosensors* **2020**, *10*, 101.

(65) Nurulkhalilah Tukimin, J. A., Yusran Sulaiman *J. Electrochem. Soc* **2018**, *165*, 258.

(66) Thanh, T. D.; Balamurugan, J.; Lee, S. H.; Kim, N. H.; Lee, J. H. *Biosens Bioelectron* **2016**, *81*, 259.

(67) Arumugasamy, S. K.; Govindaraju, S.; Yun, K. *Appl Surf Sci* **2020**, *508*, 145294.

(68) Taylor, I. M.; Patel, N. A.; Freedman, N. C.; Castagnola, E.; Cui, X. T. *Anal Chem* **2019**, *91*, 12917.

(69) Kunpatee, K.; Traipop, S.; Chailapakul, O.; Chuanuwatanakul, S. *Sens. Actuators B Chem.* **2020**, *314*, 128059.

(70) Yang, Z.; Liu, X.; Wu, Y.; Zhang, C. *Sens. Actuators B Chem.* **2015**, *212*, 457.

Chapter 2. Electro-polymerization of Au NPs/Poly-terthiophene thin-film at a micro liquid | liquid interface

2.1. Introduction

Films and coatings of NPs play an essential role in emerging technologies due to their distinctive biological,[1] opto-electrical,[2] and magnetic[3] properties. There are some different techniques to synthesis thin films, that can be classified into physical and chemical deposition.[4] In the physical deposition process, the material to be deposited is vaporized from its source and physically deposited onto the substrate.[4] Chemical deposition, on the other hand, takes advantage of a chemical reaction to self-assemble the film.[5] One popular subcategory of chemical deposition techniques is chemical vapor deposition (CVD), which is conducted by a chemical vapor precursor. Electrochemical deposition is another type of chemical deposition, in which the current flow is responsible for the film formation.[5]

Although utilizing the solid|solution interface for the electrochemical deposition has attracted a lot of attention, one possible problem of this technique is the presence of pores and roughness on the interface surface, and the frequent polishing of the surface that is required, which may affect the final result and its reproducibility.[6] Another issue with the solid|solution interface is electrode fouling as the redox reaction byproducts can be absorbed to the electrode surface and decrease its activity.[7] One applicable way to address these issues is using a liquid|liquid interface instead of a solid|liquid one.

A liquid|liquid interface is an ideal platform for the self-assembly of different species like molecules and nanoparticles.[8-9] Liquid|liquid interface is molecularly sharp and has a defect-free pristine nature, so there is no need to polish the surface that facilitates reproducibility and synthesis of free-standing film at the interface.[10] As current only depends on the charge, it is possible to push or pull the charges toward or away from the liquid|liquid interface by applying a potential. Thus, a liquid|liquid interface cannot only be used to study electroactive species but also can be used to investigate non-redox or non-electroactive ones. This advantage helps to study biological systems containing non-redox molecules like proteins.[11] Electrochemical investigation of the liquid|liquid interface helps us to fundamentally study the interface's IT and ET reactions. It also shows simplicity, selectivity, fast analysis, and inexpensive instrument cost.[12-13]

Herein, a micro-sized liquid|liquid interface was used because of some advantages over large scale interface. Some advantages of liquid|liquid micro-interface over larger interfaces are significant reduction of the ohmic potential drop, high mass transfer rate, reduction of capacitive currents, ability to sense extremely weak current and fast steady-state response.[14-16]

In this chapter, a detailed description of the experimental procedures and techniques employed is provided. The fabrication of an Au-NP/polythiophene (PT) film is reported through simultaneous electro-polymerization of terthiophene or bithiophene (TT or BT) as electron donor and $AuCl_4^-$ reduction at a micro-ITIES between w|DCE (water|1,2-dichloroethane). Three different concentration ratios of Au salt:TT (1:1, 1:2, and 1:3) and

three pH values (2, 5.5 and 8.5) were investigated. The morphology and size of the Au NPs at the ITIES were controlled by changing the applied potential, aqueous phase pH, and $KAuCl_4$:TT concentration ratio. During the experiment $AuCl_4^-$ is reductively deposited, and TT is oxidized and polymerized at ITIES leading the Au-PT film formation.

First, the instrumentation related to the electrochemical cell at the liquid|liquid interface will be described. Then the electrochemistry of the system is discussed and finally the results of the experiments will be investigated in detail.

2.2. Charge transfer processes at a liquid|liquid interface

According to the Nernst equation, the driving force for the electrochemical charge transfer (CT) is the Galvani potential difference between two phases localized at the *w*|*o* interface. The potential of the aqueous phase is called ϕ_W and that of the organic phase is called ϕ_O. The current across the interface results from CT, either simple IT, homogenous ET or heterogenous ET, Scheme 2.1. In simple IT, the Galvani potential at the interface depends on the activity of the involved species (Eq. 2.1):

$$\Delta_O^W \phi = \phi_O - \phi_W = \Delta_O^W \phi_i^0 + \frac{RT}{n_i F} \ln \frac{a_{i,O}}{a_{i,W}} \qquad (2.1)$$

Where ϕ is potential, R, T, n_i and F are gas constant, temperature in Kelvin, number of electrons transferred, and Faraday constant, respectively. a is the activity of the species involved in the redox reaction. For the heterogeneous ET, the Galvani potential depends

not only on the activity of the species in the redox reaction but also on electrochemical redox potential (Eq. 2.2):

$$\Delta_O^W \phi = \mathrm{E}^0_{\frac{\mathrm{Ox}_2}{\mathrm{Red}_2},\mathrm{org}} - \mathrm{E}^0_{\frac{\mathrm{Ox}_1}{\mathrm{Red}_1},W} + \frac{\mathrm{RT}}{\mathrm{n_1 n_2 F}} \ln \frac{\mathrm{a}_{\mathrm{Red}_1,w}\mathrm{a}_{\mathrm{Ox}_2,o}}{\mathrm{a}_{\mathrm{Ox}_1,w}\mathrm{a}_{\mathrm{Red}_2,o}} \qquad (2.2)$$

where E^0 the standard redox potential. Figure 2.1A shows a simple IT across the *w*|*o* interface by applying an external potential. Due to the applied potential, ions are forced to move across the interface. ET is another type of CT that can happen in the electrochemical system, and it can be homogenous or heterogeneous. Homogenous ET means simple IT followed by an ET, so IT happens across the interface and ET takes place in one phase, see Figure 2.1B. In heterogeneous ET, electrons move from one phase to another and ET occurs across the *w*|*o* interface, see Figure 2.1C. In this case, an electron donor from the organic phase donates an electron to the electron acceptor in the aqueous phase.

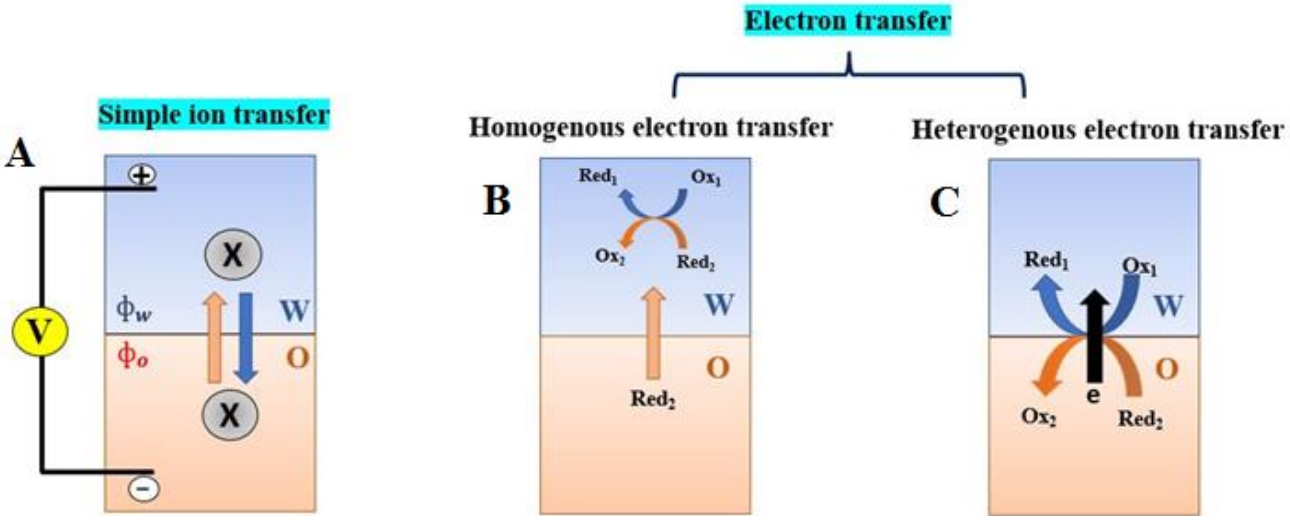

Figure 2.1 Schematic representation charge transfer processes at a liquid|liquid interface.

2.2.1. Two-electrode cell for a liquid|liquid interface

All IT and ET voltammetry measurements at the w|DCE interface were performed using a two-electrode cell. Briefly, the WE is placed in the aqueous phase and the reference/counter electrode (RE/CE) is placed in the organic phase, so that by applying potential at the WE, an electrical circuit is formed between the WE and CE. A Pt wire served as the RE/CE and was placed in the organic phase. A modified pipette holder (HEKA Electroniks) with integrated connection to a gold (Au) wire (Goodfellow Inc.) served as WE. The holder was equipped with a syringe used to maintain the micro-ITIES (25 μm in diameter) at the pipette's tip, whose tip was submerged into the organic phase.

At the interface, the TT molecule acts as electron donor and gives electron to $AuCl_4^-$, oxidizing to the cation radical of $TT^{2+\cdot}$ and $AuCl_4^-$ by receiving 3 electrons is reduced to self-assembled Au NPs. By coupling $TT^{2+\cdot}$ together through π-π conjugation, a film is formed across the interface, which will be discussed later in detail. On the other hand, Au NPs will be electrodeposited on the film. $TT^{2+\cdot}$ acts as a capping agent and sticks to the Au NPs so there will not be any available $TT^{2+\cdot}$ to transfer from the organic to the aqueous phase.

2.3. Experimental Section

2.3.1. Chemicals and Materials

Potassium tetrachloroaurate ($KAuCl_4$ >98%), hydrochloric acid (HCl >37%), sodium hydroxide (NaOH, ≥98%), trioctylphosphine (97%), bromooctane (99%), ferrocene (Fc, ≥98%), dichloromethane (CH_2Cl_2), terthiophene (TT, 99%), bithiophene (BT, 99%), and 1,2-dichloroethane (DCE, ≥99.0%) were acquired from Sigma-Aldrich and used without additional purification. Tetrakis(pentafluorophenyl)borate lithium etherate ($Li(Et_2O)_nB(C_6F_5)_4$) (>99%) was sourced from Boulder Scientific Inc. Ultrapure water from a MilliQ filtration system (>18.2 MΩ cm) was used throughout to generate aqueous solutions. In this research tetraoctylphosphonium tetrakis(pentafluorophenyl)borate ($P_{8888}TB$) ionic liquid (IL) was chosen as a supporting electrolyte in the organic phase. $P_{8888}TB$ is relatively inexpensive and strongly hydrophobic, providing a wide PPW.[17] A brief description on how $P_{8888}TB$ IL was prepared is included below.

First, tetraoctylphosphonium bromide ($P_{8888}Br$) was prepared by adding trioctylphosphine to a stoichiometric excess of 1-bromooctane under N_2 in a pressure tube (ACE glass). A stir bar was added, the vessel was sealed, and the reaction mixture stirred for ~48 h. After excess 1-bromooctane was removed under vacuum, a clear viscous liquid was obtained. This was confirmed to be $P_{8888}Br$ by ^{1}H-NMR,[18] see Figure A1 of Appendix A. Next, $P_{8888}Br$ was combined with $Li(Et_2O)_nB(C_6F_5)_4$ in 1:1 stoichiometric equivalents in a 50%/50% (v/v) H_2O/CH_2Cl_2 solution and stirred for ~24 h. The CH_2Cl_2 phase was

collected and washed 5× with 100 mL of MilliQ water. Next, the solvent phase was removed to obtain a white crystalline solid, the purity and structure of the resulting $P_{8888}TB$ were confirmed through ^{31}P- and ^{1}H- NMR,[18] see Figures A2 and A3 of the Appendix A.

2.3.2. Electrochemistry setup

In this research, three different cells were used, Cell 1, 2, and 3. In Cell 1, 10 mM HCl was added to the aqueous solution, resulting in pH = 2, Cell 2 only contained $KAuCl_4$ at pH = 5.5, and in Cell 3, 0.1 NaOH was added to the aqueous phase, leading to pH = 8.5. Figure 2.2 details the employed electrolytic cells. A CH Instruments potentiostat (model#602E) was used for recording electrochemical measurements. In the aqueous phase, $KAuCl_4$ served as supporting electrolyte and analyte, while DCE, TT, and $P_{8888}TB$ were employed as solvent, electron donor, and supporting electrolyte, respectively.

$$\mathrm{Au}\left|\mathrm{AuCl_3}\right|\begin{matrix}\text{10 mM HCl}\\ x\text{ mM }\mathrm{KAuCl_4}\\ (aq)\end{matrix}\Big\|\begin{matrix}y\text{ mM }D\\ \text{5 mM }\mathrm{P_{8888}TB}\\ (DCE)\end{matrix}\Big|\mathrm{PtTB}\left|\mathrm{Pt}\right. \qquad \text{[Cell 1]}$$

$$\mathrm{Au}\left|\mathrm{AuCl_3}\right|\begin{matrix}\\ x\text{ mM }\mathrm{KAuCl_4}\\ (aq)\end{matrix}\Big\|\begin{matrix}y\text{ mM }D\\ \text{5 mM }\mathrm{P_{8888}TB}\\ (DCE)\end{matrix}\Big|\mathrm{PtTB}\left|\mathrm{Pt}\right. \qquad \text{[Cell 2]}$$

$$\mathrm{Au}\left|\mathrm{AuCl_3}\right|\begin{matrix}\text{0.1 mM NaOH}\\ x\text{ mM }\mathrm{KAuCl_4}\\ (aq)\end{matrix}\Big\|\begin{matrix}y\text{ mM }D\\ \text{5 mM }\mathrm{P_{8888}TB}\\ (DCE)\end{matrix}\Big|\mathrm{PtTB}\left|\mathrm{Pt}\right. \qquad \text{[Cell 3]}$$

Figure 2.2 Electrolytic cells employed, where *x* and *y* correspond to the concentrations of $KAuCl_4$ and *D*, the electron donor (*i.e.*, TT or BT), respectively. The pH of Cell 2 was

roughly 5.5 (MilliQ ultrapure water), while Cells 1 and 3 were confirmed to be at pH 2 and 8.5, respectively. In each case, 5 mM of $P_{8888}TB$ was added to the organic phase as a supporting electrolyte. The double line indicates the ITIES or polarizable liquid junction.

The experiment's setup is shown in Figure 2.3. At first, a microelectrode containing a 25 µm size channel at the tip of the pipette was fabricated. The aqueous phase and $KAuCl_4$ are inserted into the micropipette and then immersed into the vial containing the organic phase. The end of the microchannel is the w|DCE interface, the place where redox reaction happens. So, the TT film electrogeneration and Au NPs electrodeposition take place across the 25 µm diameter micro interface.

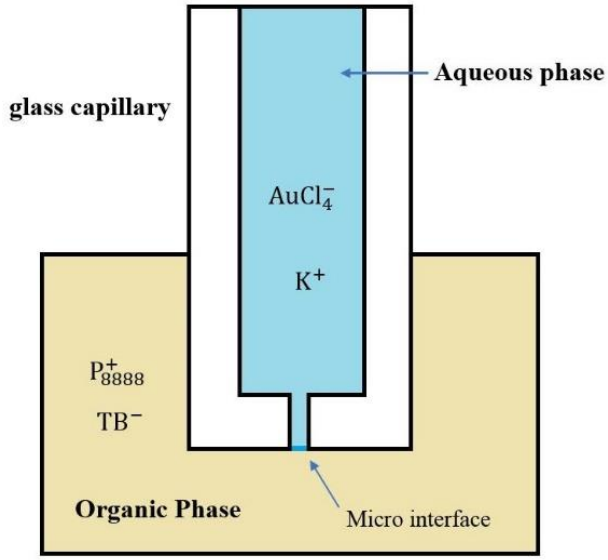

Figure 2.3 Schematic of the micropipette tip whose orifice is 25 µm in diameter and contains the aqueous phase solution of $KAuCl_4$ inside while the organic phase, including TT/BT and $P_{8888}TB$, is held outside in a small vial. The micro-ITIES is maintained at the tip of the micropipette.

2.3.3. Micropipette preparation

To generate the micropipette, a borosilicate glass capillary (1.16 mm/2.0 mm internal/external diameter) was fixed in an electric puller (PC-100-CA, Narishige, Japan). The capillary was centered within the puller's heating coil and pulled gravimetrically using a weight fixed to the bottom; whereby, two tapered tips were generated. A hand torch was then used to seal the tapered ends of the capillaries. Approximately 1.5 cm of Pt-wire (25 μm in diameter, Goodfellow Inc.) was loaded into the capillary through the open end and pushed into place in the other tapered end using a ~1 mm diameter copper wire. Under vacuum (a small hose was attached to the open end of the capillary), the Pt-wire was annealed in place using the electric puller and suspending the tapered end inside the heating coil. Next, by using increasingly fine grinding/polishing pads, including 12, 4 and 3 μm FibrMet aluminum oxide brasive discs (Buehler), a smooth cross-section was achieved and confirmed *via* visual inspection using an optical microscope. Polishing was also used to achieve a $R_g > 50$ ($R_g = r_g/a$), where r_g is the outer glass radius and a is the Pt disc radius. The Pt-wire was then etched *via* immersion in aqua regia (3:1 ratio of HCl:HNO_3) for up to 7 days, generating a 25 μm diameter microchannel.

2.4. Results and Discussion

In Figure 2.4A, the blue trace shows the CV obtained at a w|DCE micro-ITIES using Cell 1 containing 0.1 mM $KAuCl_4$ in the aqueous phase (pH = 2), acting as the analyte and supporting electrolyte, but with no TT/BT added to the DCE phase, *i.e.*, a blank CV. The

CV was acquired at a scan rate of 0.020 V s^{-1}, first scanning to positive and then negative potentials with an initial potential of 0.065 V, and positive and negative switching potentials of 0.45 and –0.25 V, respectively. The sharp increase and decrease in current at positive and negative potentials correspond to the simple transfer of K^+ and Cl^- ions from *w*→*o*, respectively. These constitute the limits of the PPW. During the negative scan from 0.45 to –0.25 V, a peak-shaped wave was observed at 0.105 V; if a charge of z = –1 is assumed, then the half-wave potential $\left(\Delta_o^w \phi_{1/2}\right)$ was calculated to be 0.133 V, which agrees well with the previous reports of the simple $AuCl_4^-$ transfer from *w*→*o*.[19-21] When scanning back from negative to positive potentials a sigmoidal shaped wave is observed in the same region and is indicative of $AuCl_4^-$ transfer back from *o*→*w*. The asymmetrical *i*-V response is owing to geometric confinement inside the micro-pipette such that IT from *w*→*o* follows a linear diffusion regime behavior and results in a peak-shaped response, in contrast, IT from *o*→*w* follows a hemispherical diffusion regime, resulting in a sigmoidal current profile.[22-24]

If the pH in the aqueous phase is increased, then a second peak appears (see Figure 2.1B) at ~0.007 V. This peak is described as the simple IT of $AuCl_{(4-\gamma)}(OH)_\gamma^-$ from *w*→*o* since at moderate to high pH $KAuCl_4$ can undergo speciation with OH^-, no attempt was made here to discriminate between the different Au-ligand species.[21, 25]

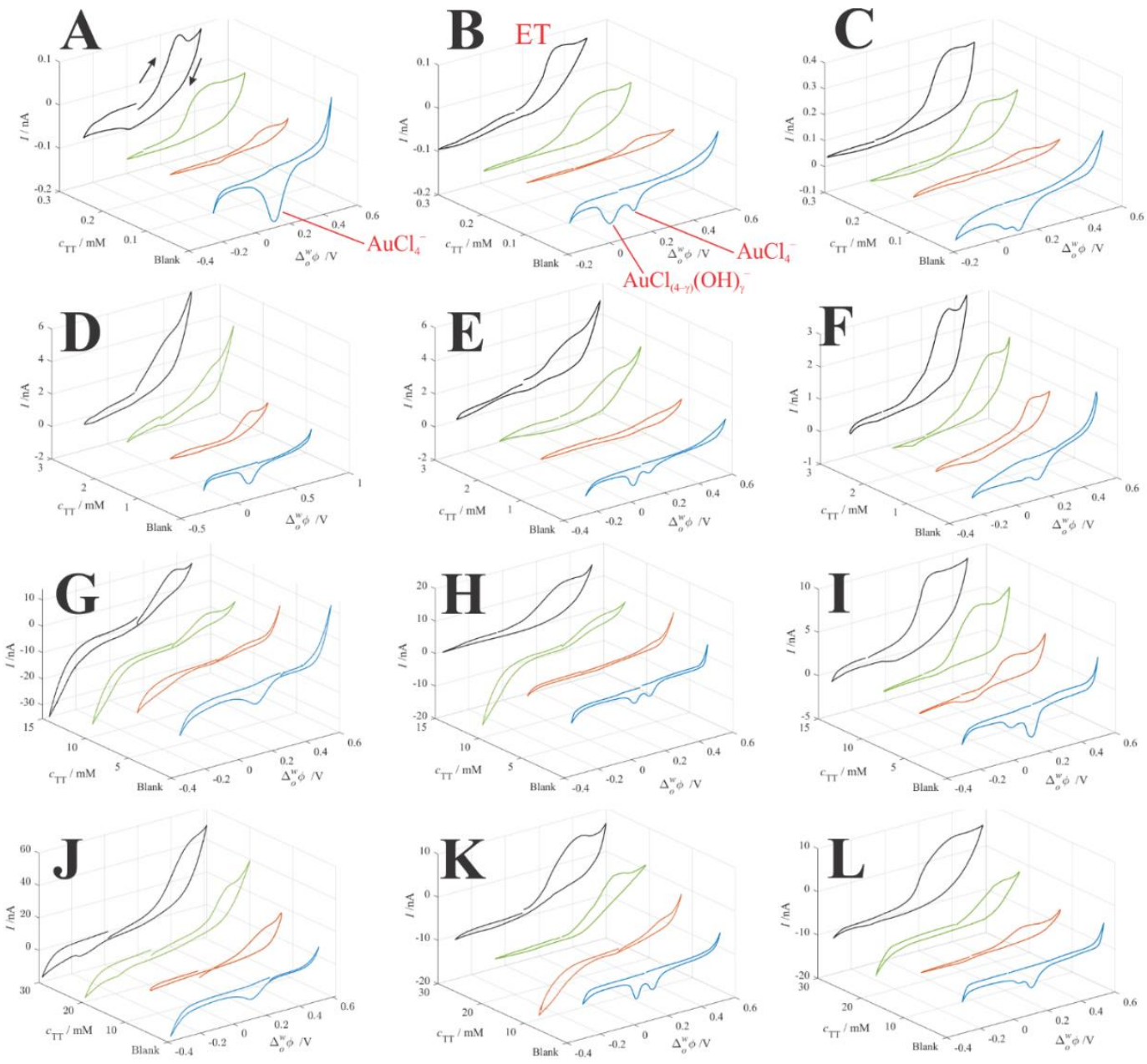

Figure 2.4 Cyclic voltammograms (CVs) recorded at the micro-ITIES interface with 0.1 (A-C), 1 (D-F), 5 (G-I), and 10 mM (J-L) of [$KAuCl_4$](aq) and such that the left-hand, middle, and right-hand columns correspond to pH 2, 5.5, and 8.5, and Cells 1, 2, and 3, respectively. CVs were recorded at a scan rate of 0.020 V s^{-1}. Arrows indicate scan direction and simple IT peaks have been labeled in red. ET = electron transfer, while Blank indicates no BT/TT added to the organic phase.

For each $KAuCl_4$ concentration tested, 1:1, 1:2, and 1:3, [$KAuCl_4$]:[TT] concentration ratios were investigated. In Figure 2.4, K with [$KAuCl_4$] = 10 mM, after the addition of TT to the organic phase, the simple IT waves of $AuCl_4^-/AuCl_{(4-\Upsilon)}(OH)_\Upsilon^-$ are replaced by a sigmoidal wave at roughly 0.4 V whose steady-state current increases concomitantly with [TT] from 9.3 nA to 22.5 and 30.4 nA, transitioning into a peak-shaped wave at [TT] = 20 and 30 mM. Indeed, at high [$KAuCl_4$]:[TT] ratios of 1:3, the *i*-V response typically takes on a peak-shaped profile for most of the conditions tested as plotted in Figure 2.4. It was hypothesized that the positive peak current is associated with ET across the ITIES between $AuCl_4^-$ (aq) and TT (org) as described through the following reaction:

$$\mathbf{6AuCl_{(4-\gamma)}(OH)_\gamma^- + 6\,\gamma\,H^+(aq) + 3TT(org) \rightarrow 6Au(s) + 3TT^{2+\cdot}\,(org) + 6(4-\gamma)Cl^-(aq) + 6\gamma H_2O(l)}$$

Here, TT acts as a 2-electron donor; it is further speculated that TT undergoes simultaneous electro-polymerization at the ITIES. To best describe the thermodynamics of TT oxidation in DCE, the redox potential of TT was measured in DCE at a 7 μm diameter carbon fiber UME as shown in Figure 2.5 and compared versus ferrocene (Fc). $E^{o',DCE}_{Fc^+/Fc}$ (*vs.* Standard Hydrogen Electrode (SHE)) in DCE is well known as 0.640 V;[26] in this way, $E^0_{TT^{2+\cdot}/TT}$ (*vs.* SHE) was calculated to be 1.20 V.

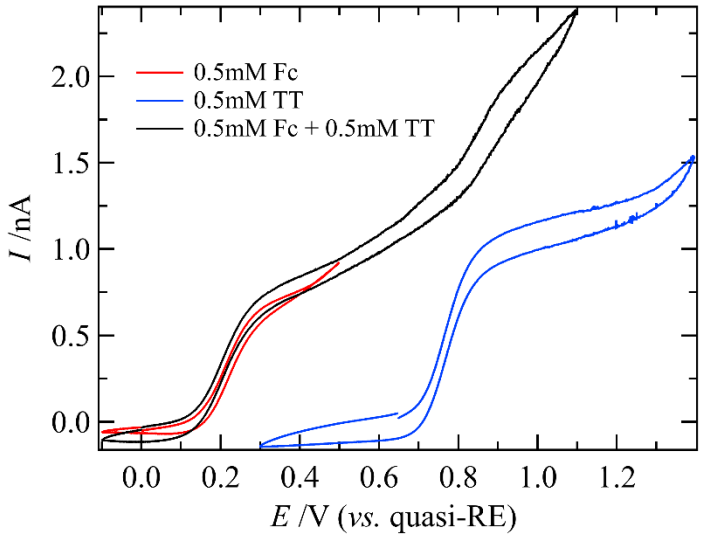

Figure 2.5 CVs recorded using a 7 μm diameter inlaid carbon fiber disk UME in DCE with 5 mM $P_{8888}TB$ as supporting electrolyte along with the concentrations of Fc and TT indicated inset.

According to the Nernst equation, the redox potential at the liquid|liquid interface can be given as follows (Eq. 2.3):

$$\Delta_{\mathrm{O}}^{\mathrm{W}}\phi = \phi_{\mathrm{o}} - \phi_{\mathrm{w}} = \Delta_{\mathrm{O}}^{\mathrm{W}}\phi_{\mathrm{i}}^{0} + \frac{\mathrm{RT}}{n_{\mathrm{i}}\mathrm{F}}\ln\frac{\mathrm{a_{i,o}}}{\mathrm{a_{i,w}}} \qquad (2.3)$$

According to Johans *et al.*[27] the potential of interfacial ET is generated by the following equation (Eq. 2.4):

$$\Delta_{\mathrm{o}}^{\mathrm{w}}\phi = \mathrm{E}_{\mathrm{Red/Ox}}^{\mathrm{o'}} - \mathrm{E}_{\mathrm{M^{o}/M^{nM}}}^{\mathrm{o'}} + \frac{\mathrm{RT}}{\mathrm{n_{Red}n_{M}F}}\ln\left(\frac{\mathrm{C_{Ox}^{\sigma}(O)^{nm}}}{\mathrm{C_{Red}^{\sigma}(O)^{nm}C_{M}^{\sigma}(W)^{n_{Red}}}}\right) \qquad (2.4)$$

where $E^{o'}_{Red/Ox}$ and $E^{o'}_{M^0/M^{nM}}$ are the formal potentials for the organic and aqueous redox couples regarding SHE in the respective phases. By considering reaction 1 and Eq. 2.3 we would reach the following equations:

$$\Delta^{w}_{o}\phi_{ET} = [E^{o'}_{TT^{2+\cdot}/TT}]^{DCE} - [E^{o'}_{AuCl_4^-/Au}]^{H_2O} + \frac{RT}{n_{(TT^{2+\cdot}/TT)}n_{(AuCl_4^-/Au)}F}\ln\left(\frac{[Cl^-]^{6(4-\gamma)}[TT^{2+\cdot}]^3}{[AuCl_{(4-\gamma)}(OH)_\gamma^-]^6[TT]^3[H^+]^{6\gamma}}\right) \quad (2.5)$$

$$\Delta^{w}_{o}\phi_{ET} = [E^{o'}_{TT^{2+\cdot}/TT}]^{DCE} - [E^{o'}_{\frac{AuCl_4^-}{Au}}]^{H_2O} + \frac{RT}{3F}\left[\ln\left(\frac{[Cl^-]^{6(4-\gamma)}[TT^{2+\cdot}]^3}{[AuCl_{(4-\gamma)}(OH)_\gamma^-]^6[TT]^3}\right) - \ln[H^+]^{6\gamma}\right] \quad (2.6)$$

$$\Delta^{w}_{o}\phi_{ET} = [E^{o'}_{TT^{2+\cdot}/TT}]^{DCE} - [E^{o'}_{AuCl_4^-/Au}]^{H_2O} + \frac{RT}{3F}\ln\left(\frac{[Cl^-]^{6(4-\gamma)}[TT^{2+\cdot}]^3}{[AuCl_{(4-\gamma)}(OH)_\gamma^-]^6[TT]^3}\right) - \frac{RT}{3F}\ln[H^+]^{6\gamma}$$

(2.7)

As the highlighted term can be considered as a constant term for all the experiments, it can be neglected, and the following equation would be achieved (Eq. 2.8):

$$\Delta^{w}_{o}\phi_{ET} \approx [[E^{o'}_{TT^{2+\cdot}/TT}]^{DCE} - [E^{o'}_{AuCl_4^-/Au}]^{H_2O} - \frac{(0.059\ V)}{3}\log([H^+]^{6\gamma}) \quad (2.8)$$

In a low concentration and dilute solution γ =1 and this equation simplified (Eq. 2.9):

$$\Delta^{w}_{o}\phi_{ET} \approx [E^{o'}_{TT^{2+\cdot}/TT}]^{DCE} - [E^{o'}_{AuCl_4^-/Au}]^{H_2O} + \frac{0.059\ V}{3}pH \quad (2.9)$$

Based on this equation, the ET potential depends on the standard redox potential of TT and $AuCl_4^-$, and pH of the solution. By using $E^0_{TT^{2+\cdot}/TT}$ which was calculated before,

1.20 V, and the standard reduction potential of $AuCl_4^-$ in water ($E^{o,H_2O}_{AuCl_4^-/Au}$ = 1.002 V),[28] one can calculate the approximate liquid|liquid, interfacial ET potential $\left(\Delta^w_o\phi_{ET}\right)$ by using equation (2.9).[19, 26, 29-30]

In this study, $\Delta^{w}_{o}\phi_{ET}$ was calculated in three different pH, so that, $\Delta^{w}_{o}\phi_{ET}$ was 0.24, 0.31, and 0.37 V for the aqueous pH regimes 2, 5.5, and 8.5 tested in Figure 2.1, respectively. These values indicate the overall favourability of the reaction and agree well with the observed position of ET. For example, in Figure 2.1G, H, and I, with [TT] = 15 mM, the peak potential for the proposed ET was found to be 0.38, 0.37, and 0.31 V, respectively, which agree nominally with the calculated values.

Figure 2.6 represents the optical images before and after running one CV cycle by employing Cell 1 and using a sample containing 5 mM $KAuCl_4$ and 15 mM terthiophene. It is clear before running CV, there are no NPs around the microchannel; however, after applying potential and running a CV cycle, some NPs near and above the microchannel were created and it is assumed that these are Au NPs or the film formed at the interface. The mechanism of how these NPs move to the top of the microchannel is not precisely clear yet, but it is believed this happens because of the strong positive potential gradient toward the aqueous electrode.

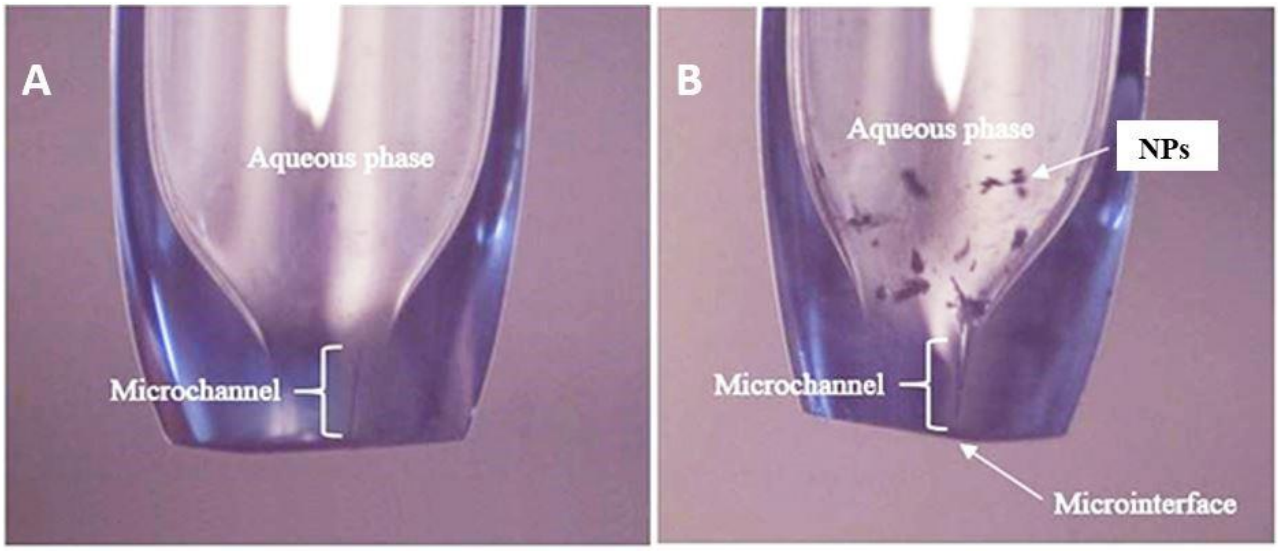

Figure 2.6 Photos taken of the tip and micropipette using an 18-megapixel CCD camera equipped with a 12× magnification lens assembly (Navitar) before (A) and after (B) the CV. Scan rate was 0.020 V s^{-1} using Cell 1 with [$KAuCl_4$] = 5 [TT] = 15 mm.

SEM was carried out to investigate the film formation across the liquid|liquid interface. Thus, after running one CV cycle, one droplet was ejected from the tip of the microelectrode over an Indium Tin Oxide (ITO) glass surface, and it was directly inserted into the SEM chamber. SEM of different [$KAuCl_4$]:[TT] ratios were done, and the SEM result of sample in Cell 1 (pH=2) with [$KAuCl_4$]:[TT] 1:1 is shown. Figure 2.7A shows film formation throughout the ejected droplet across the ITO glass. Figure 2.7B is a zoomed in version and the film formation is more obvious.

To see the Au NPs, we go further and Figure 2.7C shows the film containing Au NPs at the substrate. The presence of the Au NPs in all the samples was confirmed by running the EDX technique. Figure 2.8 shows the EDX results of three spots selected from the

Figure 2.7C. Points 1 and 2 are inside the film and point 3 is outside of the film over the ITO surface. According to the EDX result at point 3 there were no Au NPs and it mainly contains silicon. However, the two other points contain a high Au content, confirming the presence of what are likely Au particles on the film. Point 2 is almost entirely Au and likely an Au micro particle.

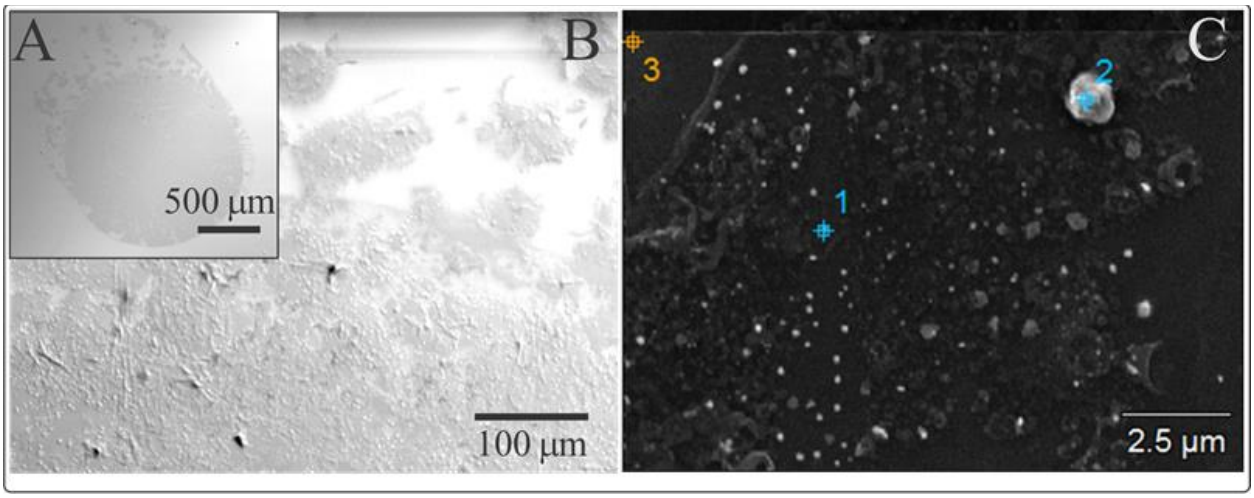

Figure 2.7 SEM images of Au NPs and PT film generated using [$KAuCl_4$] = 1 mM and [TT] = 1 mM by using Cell 1. (A) film formation throughout the ejected droplet across the ITO glass. (B) 5x zoomed in pic (C) 200x zoomed in pic, points 1 and 2 are inside the film and point 3 is on the ITO surface.

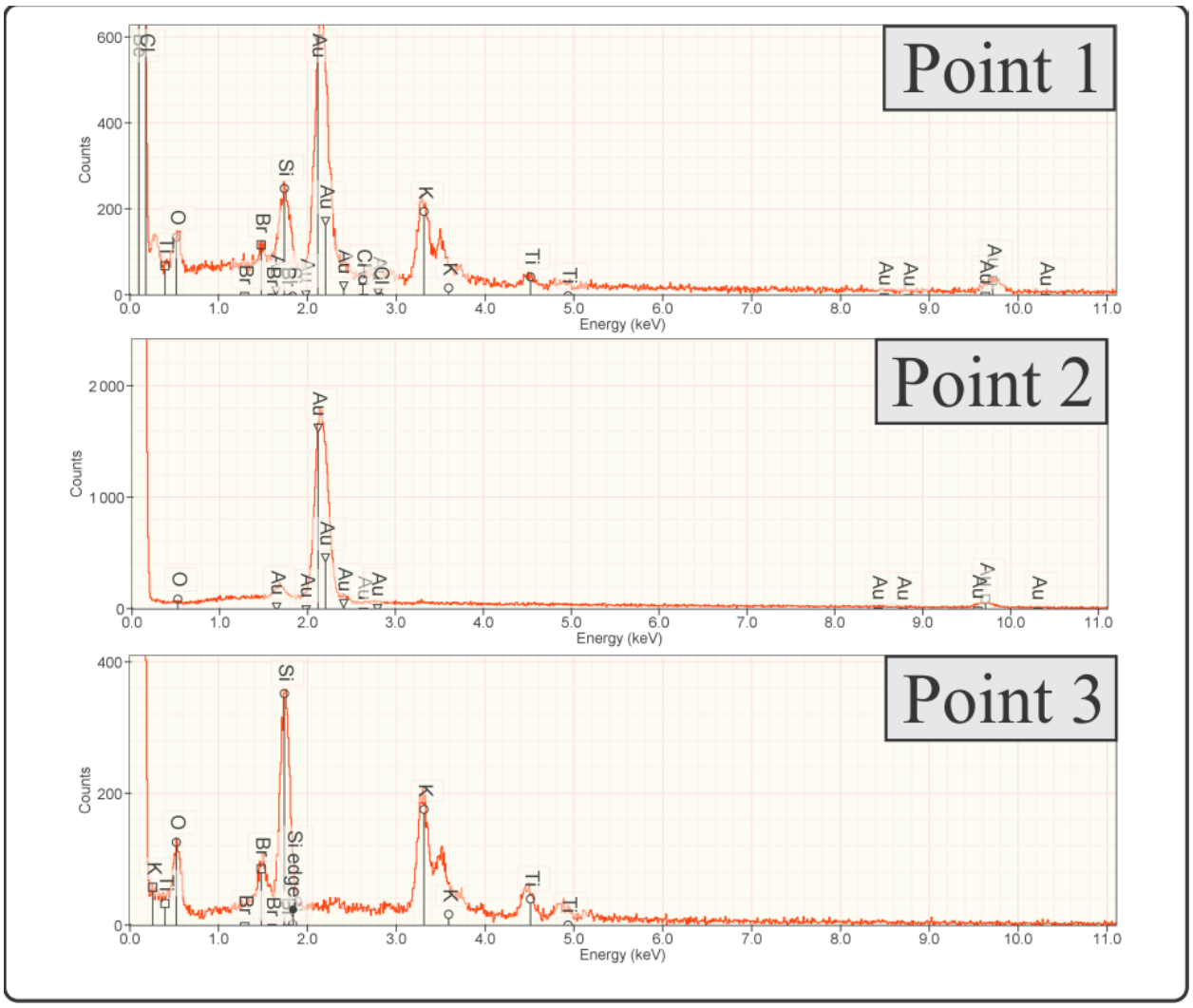

Figure 2.8 EDX spectra of three different points of Au NPs and PT film generated with [$KAuCl_4$] = 1 mM and [TT] = 1 mM by using Cell 1.

To investigate the electrodeposition and the morphology of the Au NPs, the TEM technique was carried out. To do so, a droplet was ejected from the end of the micropipette onto a TEM grid, rinsed with MilliQ water and imaged using TEM (see Figure 2.9). Various process parameters can influence the growth of the Au NPs, but here all the process parameters were kept constant, except the pH to investigate its effect on the growth

mechanism and morphology of Au NPs and in all samples the concentration ratio of Au:TT was 1:3.

According to the result, change in pH leads to variation of the Au NPs morphology. Based on the histogram, which is a graphical representation of some random particle length by Igor software, at pH 2 and 5.5 the average sizes of the Au NPs were 33±4 and 110±10 nm, respectively, and they were cubic in shape. However, at pH 8.5 the average size of NPs increased to 314±13 nm and the morphology changed to a flower-like shape. It means that at lower pH, particles are smaller and monodisperse relative to at higher pH. The formation of flower-like shape particles agrees with a recent study by Nishi and co-workers. They generated Janus-type Au/PT NPs at a water|IL interface and studied the particle growth at the mm-sized ITIES.[31]

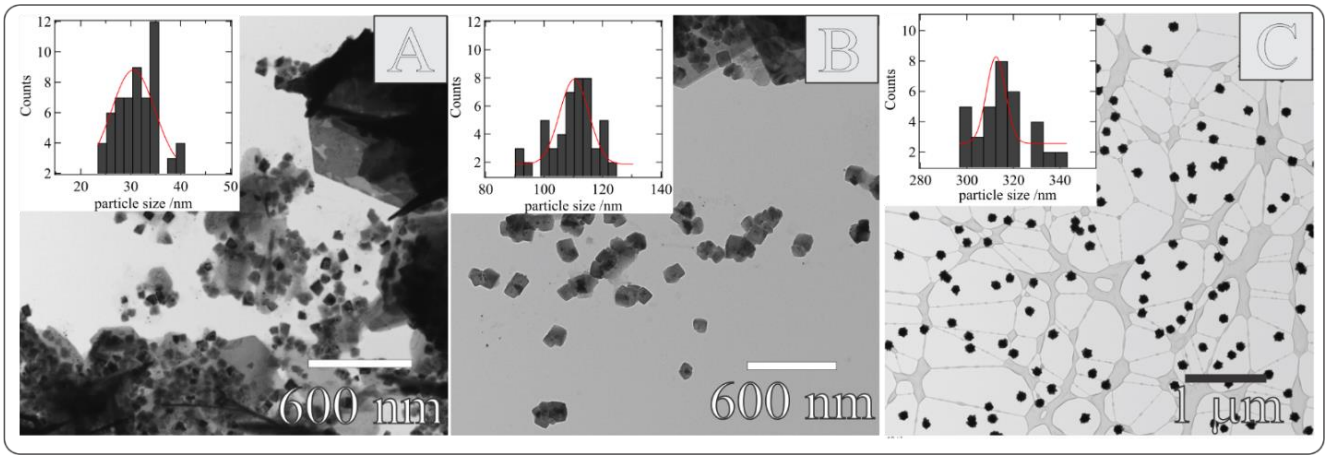

Figure 2.9 TEM micrographs of Au NPs and PT generated using [$KAuCl_4$] = 1 mM and [TT] = 3 mM at pH (A) 2, (B) 5.5, and (C) 8.5.

Next, all the experiments were repeated by using BT instead of TT as the electron donor. Contrary to TT, by adding BT to the organic phase, the transfer peak proposed to $AuCl_4^-$ does not disappear and no ET peak wave emerged in positive scanning wave. So, it is assumed that no ET happens between the BT and $AuCl_4^-$ and no film formed across the interface. Figure 2.10 shows the CV result by using samples containing 5 mM of $AuCl_4^-$ in different concentrations of BT in Cell 1.

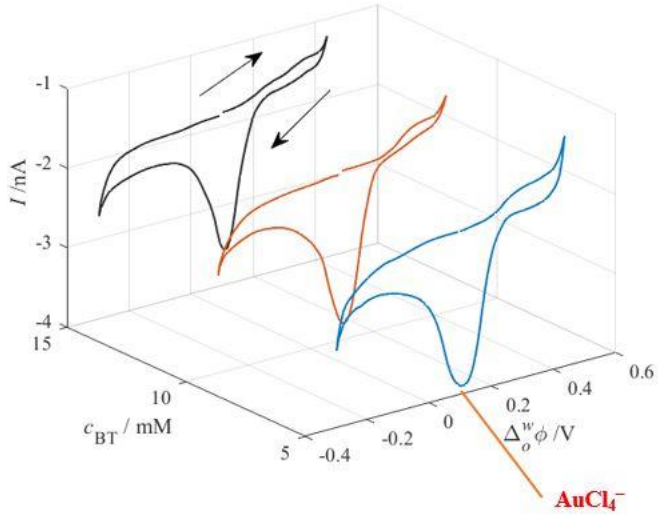

Figure 2.10 CVs recorded at the micro-ITIES interface, using Cell 1 (pH 2) with [$KAuCl_4$](aq) = 5 mM and (BT) at varying concentrations in the DCE phase as indicated on the *y*-axis. CVs were recorded at a scan rate of 0.020 V s^{-1}. Arrows indicate scan direction and simple IT peak of $\mathbf{AuCl_4^-}$ has been labeled in red.

The reason BT does not form a film across the liquid|liquid interface is unclear, but we assumed that as the oxidation potential of TT is lower than that of BT,[32] the electrochemical growth of TT polymer film is easier than that of BT.

2.5. References

1. Kaushik, A. C.; Bharadwaj, S.; Kumar, S.; Wei, D.Q. *Sci. Rep.* **2018**, *8*.

2. Sujit Kumar Ghosh, T. P. *Chem Rev* **2007**, *107*, 4797.

3. Lisjak, D.; Mertelj, A. *Prog Mater Sci* **2018**, *95*, 286.

4. Shang, S. M.; Zeng, W. *Smart-Textiles Developers*, Woodhead Publishing **2013**, 4, 92.

5. Quero, J. M.; Perdigones, F.; Aracil, C. *Smart Sensors and MEMs* **2018**, 291.

6. Xiong, B.; Li, J.; He, C.; Tang, X.; Lv, Z.; Li, X.; Yan, X. *Mater. Res. Express* **2020**, *7*, 115013.

7. Barek, J. *Chemosensors* **2021**, *9*, 12.

8. Scanlon, M. D.; Smirnov, E.; Stockmann, T. J.; Peljo, P. *Chem Rev* **2018**, *118*, 3722.

9. Olaya, A. J.; Schaming, D.; Brevet, P.F.; Nagatani, H.; Zimmermann, T.; Vanicek, J.; Xu, H.-J.; Gros, C. P.; Barbe, J.M.; Girault, H. H. *J Am Chem Soc* **2011**, *134*, 498.

10. S Samuel G. Booth, R. A. W. D. *J. Phys. Chem. C* **2015**, *119*, 23295.

11. Vagin, M. Y.; Trashin, S. A.; Ozkan, S. Z.; Karpachova, G. P.; Karyakin, A. A. *J Electroanal Chem* **2005**, *584*, 110.

12. Rudnicki, K.; Sobczak, K.; Borgul, P.; Skrzypek, S.; Poltorak, L. *Food Chem.* **2021**, *364*, 130417.

13. Borgul, P.; Pawlak, P.; Rudnicki, K.; Sipa, K.; Krzyczmonik, P.; Trynda, A.; Skrzypek, S.; Herzog, G.; Poltorak, L. *Sens. Actuators B Chem.* **2021**, *344*, 130286.

14. Li, Q.; Xie, S.; Liang, Z.; Meng, X.; Liu, S.; Girault, H. H.; Shao, Y. *Angew. Chem. Int. Ed.* **2009**, *48*, 8010.

15. Stockmann, T. J.; Ding, Z. *J. Electroanal. Chem.* **2010**, *649*, 23.

16. Liu, S.; Li, Q.; Shao, Y. *Chem. Soc. Rev.* **2011**, *40*, 2236.

17. Stockmann, T. J.; Ding, Z. *J Phys Chem B* **2012**, *116*, 12826.

18. Stockmann, T. J.; Boyle, P. D.; Ding, Z. *Catal Today* **2017**, *295*, 89.

19. Moshrefi, R.; Suryawanshi, A.; Stockmann, T. J. *Electrochem Commun* **2021**, *122*, 106894.

20. Uehara, A.; Booth, S. G.; Chang, S. Y.; Schroeder, S. L. M.; Imai, T.; Hashimoto, T.; Mosselmans, J. F. W.; Dryfe, R. A. W. *J Am Chem Soc* **2015**, *137*, 15135.

21. Uehara, A.; Chang, S.-Y.; Booth, S. G.; Schroeder, S. L. M.; Mosselmans, J. F. W.; Dryfe, R. A. W. *Electrochim Acta* **2016**, *190*, 997.

22. Liu, S.; Li, Q.; Shao, Y. *Chem. Soc. Rev.* **2011**, *40*, 2236.

23. Stockmann, T. J.; Noel, J.-M.; Abou-Hassan, A.; Combellas, C.; Kanoufi, F. *J. Phys. Chem. C* **2016**, *120*, 11977.

24. Burgoyne, E. D.; Molina-Osorio, A. F.; Moshrefi, R.; Shanahan, R.; McGlacken, G. P.; Stockmann, T. J.; Scanlon, M. D. *Analyst* **2020**, *145*, 7000.

25. Usher, A.; McPhail, D. C.; Brugger, J. *Geochim Cosmochim Acta* **2009**, *73*, 3359.

26. Méndez, M. A.; Partovi-Nia, R.; Hatay, I.; Su, B.; Ge, P. Y.; Olaya, A.; Younan, N.; Hojeij, M.; Girault, H. H. *Phys. Chem. Chem. Phys.* **2010**, *12*, 15163.

27. Christoffer Johans, R. L., Kyosti Kontturi a, David J. Schiffrin *J Electroanal Chem* **2000**, *488*, 99.

28. William, M. H.; Lide, R. D; Bruno, T. J. *CRC Handbook of Chemistry and Physics*; **2021**, 8.20.

29. Trojánek, A.; Langmaier, J.; Samec, Z. *Electrochem. commun.* **2006**, *8*, 475.

30. Johans, C.; Lahtinen, R.; Kontturi, K.; Schiffrin, D. J. *J. Electroanal. Chem.* **2000**, *488*, 99.

31. Nishi, N.; Yajima, I.; Amano, K. I.; Sakka, T. *Langmuir* **2018**, *34*, 2441.

32. Y. Wei, C.-C. C., J. Tian, G.W. Jang, K.F. Hsueh *Chem Mater* **1991**.

Chapter 3. Electrochemical detection of dopamine using modified ultramicroelectrodes with $C_{10}C_{10}$BisDTF monomer and $KAuCl_4$

3.1. Introduction

In this section, an electrochemical sensor has been developed for DA detection. DA or 3,4-dihydroxyphenylethylamine, consists of a central benzene ring having two hydroxyl groups (catechol) attached to a monoamine by an aliphatic ethylene linker (Figure 3.1). DA is a catecholamine neurotransmitter (neurotransmitters are chemical substances in the human body, responsible as a chemical messenger from one nerve cell to another). DA is present in both the brain and nervous system, and affects basic behaviors such as movement, cognition, and timing.[1] DA also is a biological indicator for a debilitating ailment, severe mental disorder, drug addiction and some diseases.[2-4] It is believed that inappropriate function of DA can lead into some diseases such as parkinson and schizophrenia, and up to now there is no effective long-term cure for it.[2,3]

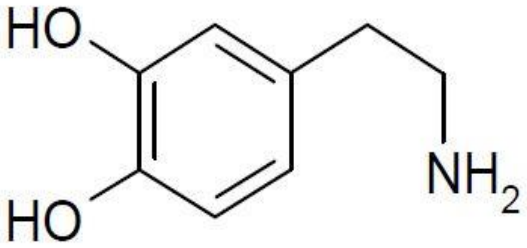

Figure 3.1 Chemical structure of DA

DA monitoring can help investigate its physiological function and eventually develop methods to control its level and effects. So, it is not surprising that finding a method with fast response time and able to precisely measure DA levels has been the focus of much recent research work. High-Performance Liquid Chromatography (HPLC),[5] UV-vis,[6] flow injection,[7] and electrochemical methods[8] are some analytical techniques that have been reported for DA detection.

3.1.1. Electrochemical detection of dopamine

As DA is electroactive, the oxidation of DA can be investigated by using electrochemical techniques. There has been much interest in developing electrochemical sensors because they are easy to employ, inexpensive to manufacture, and present high sensitivity and selectivity.[9-10] Another crucial feature of electrochemical sensors, is that they can be directly used to study living organism without significantly damaging the tissue.[11] The main problem with the electrochemical detection of DA is the coexistence of some interfering biological matrixes like ascorbic acid which has almost the same oxidization potential with DA and interferes with its detection.[12] So, unmodified electrochemical electrodes suffered from weak selectivity and sensitivity due to overlap of voltammetric responses.

Some of the electrochemically modified electrodes for DA detection are carbon-fiber UMEs,[13] carbon nanotubes modified GCEs,[14-15] surfactant modified electrodes,[16] and multilayer graphene nanoflake films.[17] Nanoparticle-based electrodes have gotten a lot of

attention recently because of their intrinsic electrocatalytic nature, which allows them to speed up the rate of ET, enhancing the sensor's selectivity towards DA.

Electrochemical methods usually are conducted with electrode surface modification. Here the surface modification of a carbon fiber UME was done by $C_{10}C_{10}$BisDTF monomer, shown in Figure 3.2, followed by $AuCl_4^-$. $C_{10}C_{10}$BisDTF monomer was supplied by the Bodwell group in the Chemistry department of Memorial University.

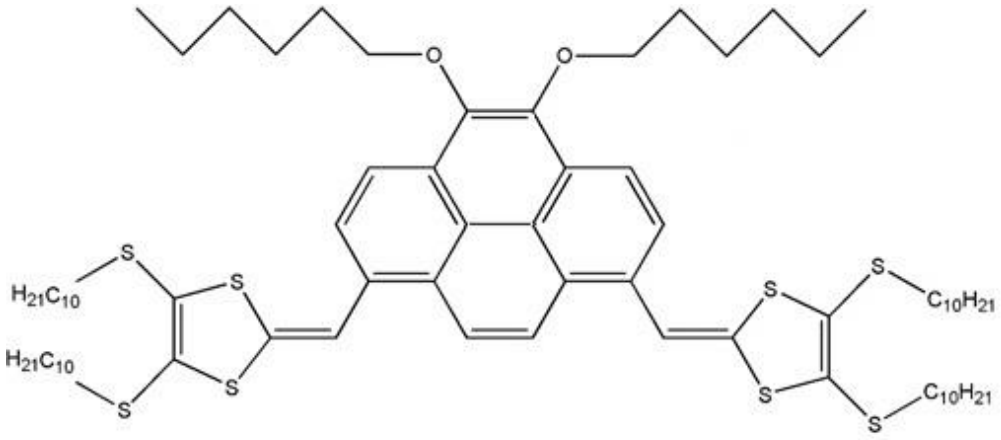

Figure 3.2 Chemical structure of 4,5-didecoxy-1,8-bis(dithiafulvenyl)pyrene ($C_{10}C_{10}$bisDTF) monomer

3.2. Experimental Section

3.2.1. Carbon-fiber electrode fabrication:

After achieving the sealed tapered end capillary as mentioned before, approximately 1.5 cm carbon fiber (7µm in diameter) was loaded into the capillary from the tapered end. Under vacuum the carbon fiber was annealed in place using the electric puller equipped with a heating coil. A smooth cross-section of the capillary was achieved by grinding/polishing with FibrMet Abrasive discs from Buehler company. Then the capillary was filled with charcoal and a copper wire was placed from the open end. The final step was affixing the copper wire inside the charcoal-filled capillary with proper tape (See Figure 3.3).

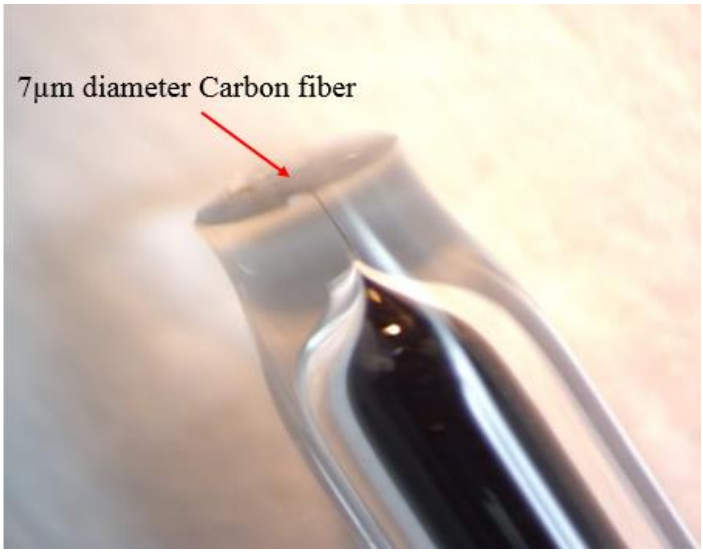

Figure 3.3 Carbon fiber UME tip whose orifice is 7 µm in diameter

3.2.2. Electrochemistry setup

Electrochemical measurements performed by a CH Instruments potentiostat (model#602E). For the film electro-generation and Au NPs electrodeposition, a two-electrode cell was used and for the DA and ascorbic acid detection a three-electrode cell configuration was employed. The cell included of RE, WE and a counter/auxiliary electrode. In the two-electrode system usually a Pt-wire was employed, while in a three-electrode configuration Ag/AgCl acts as RE. As DA is easily oxidized, all the experiments were conducted with freshly prepared DA solutions. CVs were carried out in a suitable potential range (–0.20 to 1.80 V for film electrogeneration and 0.0 to 0.95 V for Au NPs electrodeposition) in all the experiments and at the room temperature (25 °C).

3.2.3. Electrochemical surface modification of the UME

The UME surface modification was done in two steps: 1) film electrogeneration with $C_{10}C_{10}$BisDTF monomer; 2) Au NPs electrodeposition by using $KAuCl_4$. Figure 3.4 shows the first step for surface modification of the carbon fiber UME in which it was immersed in a vial containing $C_{10}C_{10}$BisDTF monomer as an electron donor. The interface between solid and solution is the carbon fiber surface, which is 7 μm in diameter (38.46 μm^2 area).

The film electrogeneration was accomplished by running a CV cycle in a sample containing 3 mM $C_{10}C_{10}$BisDTF monomer in DCE. Figure 3.5 presents the CV acquired at a scan rate of 0.020 V s^{-1}, first scanning to positive and then toward negative potentials with an initial potential of 1.50 V, and the potential limits were 1.80 and –0.20 V. SEM

was employed to confirm the film formation across the solid-solution interface, see Figure 3.6.

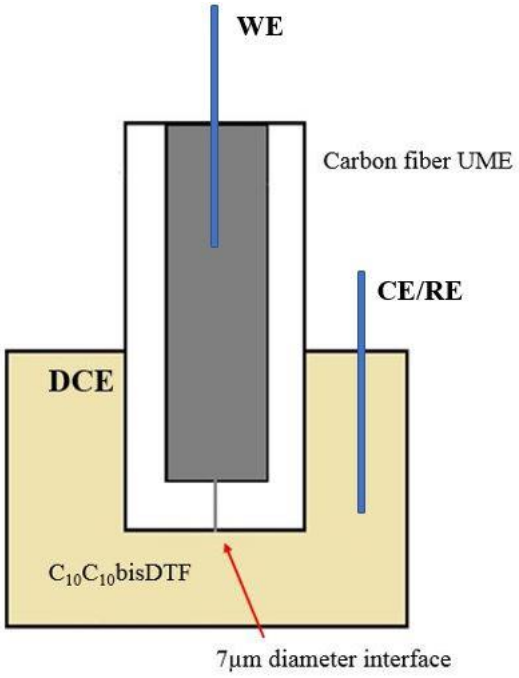

Figure 3.4 Schematic of the carbon fiber UME tip whose orifice is 7 μm in diameter, inserted in the organic phase, including $C_{10}C_{10}$BisDTF monomer and DCE as a solvent in a small vial.

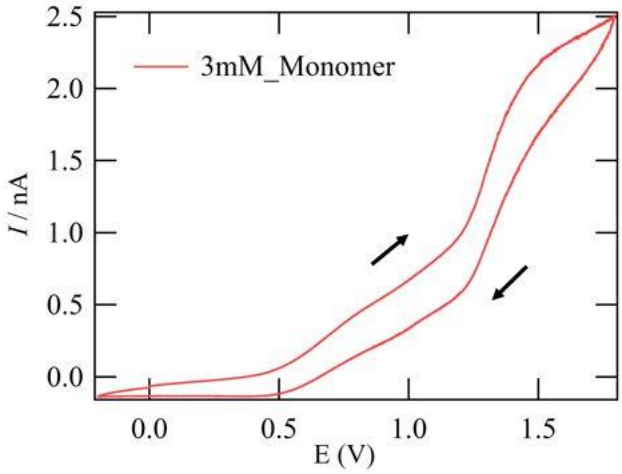

Figure 3.5 the carbon-fiber UME interface using a sample containing 3 mM $C_{10}C_{10}$BisDTF monomer in DCE. Arrows indicate scan direction

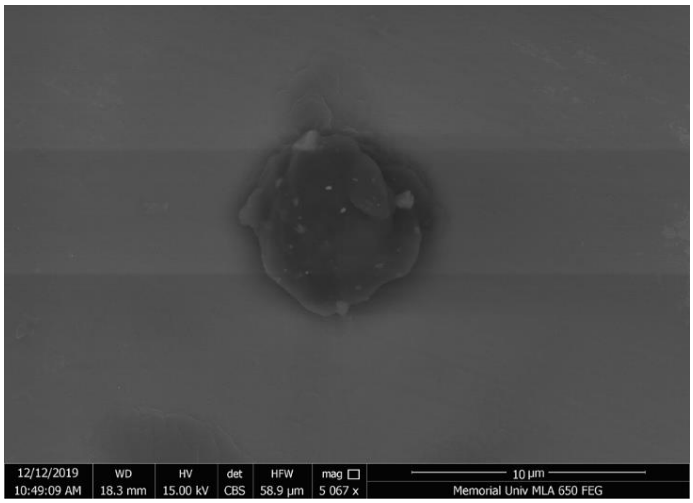

Figure 3.6 SEM micrograph of an electrogenerated film using a sample containing 3 mM $C_{10}C_{10}$BisDTF monomer in DCE

In the second step, the modified electrode was immersed in an aqueous phase containing $KAuCl_4$ as an analyte and source of gold particle. Figure 3.7 shows a schematic of the used setup.

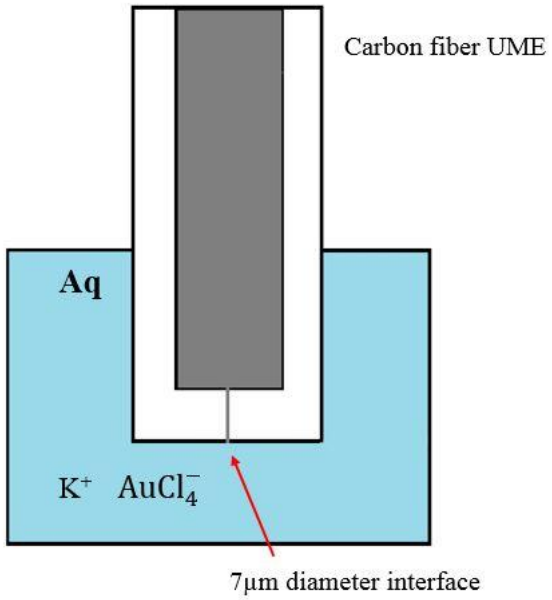

Figure 3.7 Schematic of the carbon fiber UME tip whose orifice is 7 µm in diameter, inserted in the aqueous phase, including $KAuCl_4$ in a small vial

By running 10 cycles of CV in the presence of 1 mM of $KAuCl_4$ in the aqueous phase, Au NPs electrodeposited on the modified UME surface. Figure 3.8 shows one CV cycle, in which the initial potential is 0.8 V and then it goes forward to positive potentials till 0.95 V, right edge, then in the reverse direction, it moves toward negative, reaching the left edge at 0 V and then coming back to the initial point. Figure 3.9 presents the SEM result, showing the electrodeposition of the Au NPs across the UME surface.

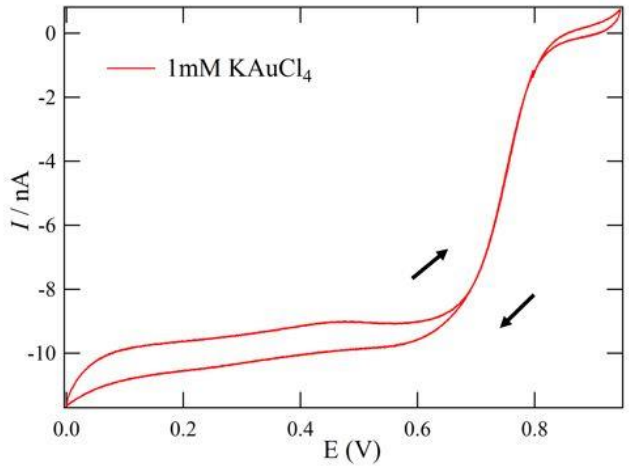

Figure 3.8 CV recorded at the carbon-fiber UME interface using a sample containing 1 mM $KAuCl_4$ in aqueous phase. Arrows indicate scan direction

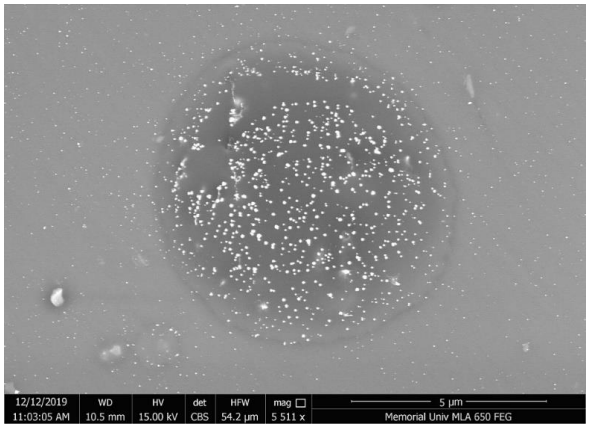

Figure 3.9 SEM micrograph of electrodeposited Au NPs using sample containing 1 mM $KAuCl_4$ in aqueous phase

3.3. Result and discussion

After surface modification of the carbon-fiber UME with polymerized $C_{10}C_{10}$BisDTF followed by $KAuCl_4$, CVs were carried out by using a sample containing DA and ascorbic acid in an aqueous phase. To compare the effect of surface modification on the sensitivity of the electrode, three different experiments were run: 1) blank solution with unmodified UME, 2) 1 mM DA solution with unmodified UME, and 3) 1 mM DA solution with modified UME, see Figure 3.10 The initial potential is 0.1 V, and the right and left edges limited with 1 and 0 V, respectively. According to the result, by running CV in a blank solution, there is no steady-state current achieved, red curve. By adding 1 mM of DA to the aqueous phase and using an unmodified UME, a 2.5 nA steady-state current is observed, black curve. However, by using modified UME the steady-state current increased to 3.7 nA, blue curve, showing that the surface modification increased the sensitivity of the UME toward DA detection.

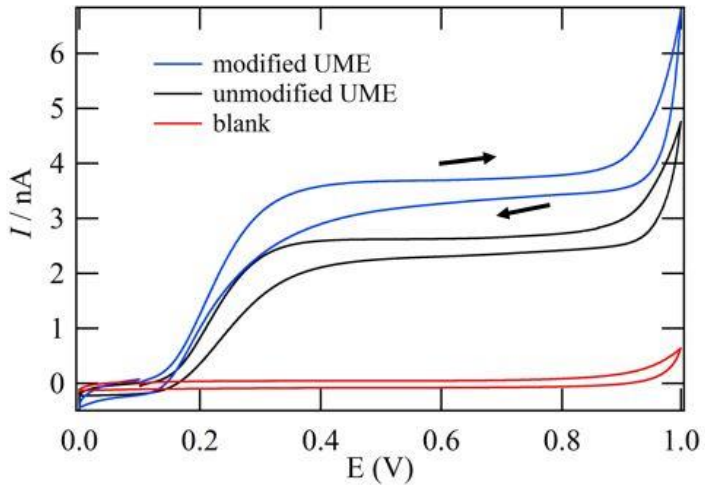

Figure 3.10 CVs recorded at the carbon-fiber UME interface to sense 1 mM DA in aqueous phase. Arrows indicate scan direction.

The same experiment was carried out towards ascorbic acid detection. Figure 3.11 indicates the CV results of unmodified and modified UME in the aqueous phase containing 1 mM ascorbic acid. According to the CVs, although no steady-state current was achieved in blank solution, a steady-state current appeared in positive scanning wave by adding 1 mM ascorbic acid to the aqueous phase. The steady-state current of modified UME was higher than the unmodified, implying sensitivity enhancement by surface modification.

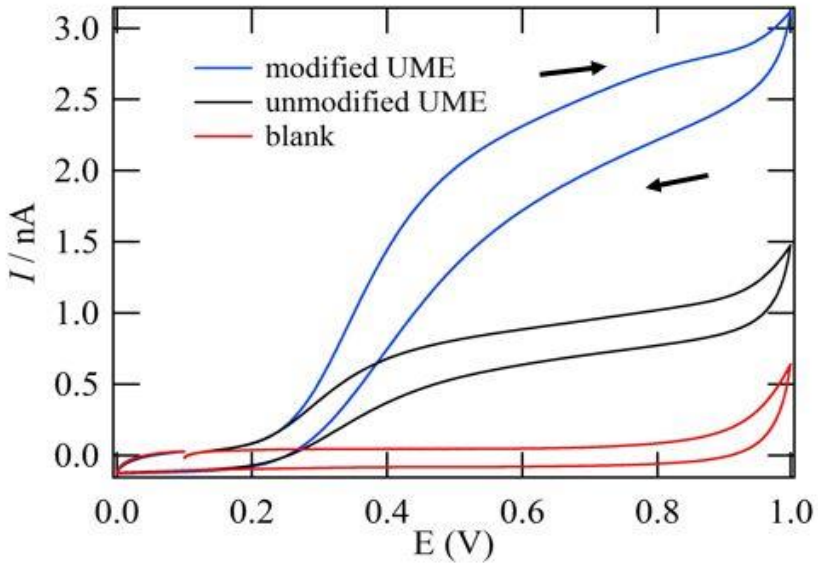

Figure 3.11 CVs recorded at the carbon-fiber UME interface to sense 1 mM ascorbic acid in aqueous phase. Arrows indicate scan direction

The next try was the surface modification of UME with different concentrations of $KAuCl_4$ to investigate the effect of electrodeposited Au NPs on ascorbic acid detection. Figure 3.12 presents the steady-state current signal vs. ascorbic acid concentration and linear regression traces (solid lines) are calibration curves. To do so, three different concentrations of $KAuCl_4$, 1, 5 and 10 mM, were employed to sense ascorbic acid in a

concentration range between 0.01 to 10 mM. The R^2 values, which is called fitting error and represent the proportion of the variance, were 0.969, 0.962 and 0.984, for 1, 5 and 10 mM $KAuCl_4$, respectively. This error is relatively low, indicating high sensitivity of modified UME toward ascorbic acid detection.

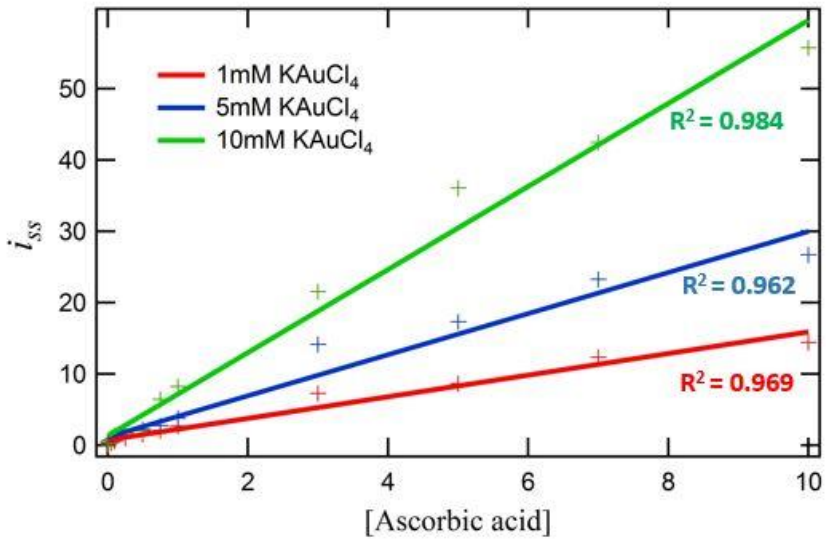

Figure 3.12 Current signal (nA) versus [ascorbic acid] plotted for UME modified by using different concentrations of $KAuCl_4$ in aqueous phase. The solid lines are the linear regression analysis, while R^2 shows the measured fitting error.

Unfortunately, because of supply limitation of the $C_{10}C_{10}$BisDTF monomer precursor further UME surface modification was not possible, and the experiment inevitably has been stopped. However, by supplying more $C_{10}C_{10}$BisDTF monomers, the electrochemical DA detection investigation would have continued.

3.4. Conclusion

Herein, we investigated the reproducible generation of Au NPs and Au-NP/PT film through simultaneous electro-polymerization of TT at the micro-ITIES as well as electrochemically modified UME to sense DA and ascorbic acid. In this study (TT/BT) and $KAuCl_4$ acted as electron donor and source of gold nanoparticles, respectively. During the experiment $AuCl_4^-$ was reduced to electrodeposited Au NPs at the ITIES, and TT was oxidized and polymerized at the ITIES leading to Au-PT film formation. We studied three different concentration ratios of Au salt:TT and three pHs of the aqueous phase to investigate the effect on the film formation across the interface. According to the results, by changing the $KAuCl_4$:TT concentration ratio the $AuCl_4^-/AuCl_{(4-Y)}(OH)_Y^-$ simple IT peak varied to interfacial ET between TT and Au salt. Moreover, by increasing pH, Au NPs morphology changed from cubic to star-like shape and their size increased. Probably the resulted film can be scaled up to use as a modified substrate surface for the industry. For the second part of the experiment, we conducted a surface modification of UME with $C_{10}C_{10}$bisDTF monomer and followed by $KAuCl_4$ for DA detection. At first, we showed that the modified UME has a higher selectivity of DA and ascorbic acid regarding unmodified UME. Then the effect $KAuCl_4$ concentration toward ascorbic acid detection has been studied.

3.5. References

1. Berke, J. D. *Nat Neurosci* **2018**, *21*, 787.

2. Phani, S.; Loike, J. D.; Przedborski, S. *Parkinsonism Relat. Disord.* **2012**, *18*, S207.

3. Seeman, P. *Eur Neuropsychopharmacol* **2013**, *23*, 999.

4. Covey, D. P.; Dantrassy, H. M.; Yohn, S. E.; Castro, A.; Conn, P. J.; Mateo, Y.; Cheer, J. F. *Neuropsychopharmacol* **2018**, *43*, 2056.

5. Chen, F.; Fang, B.; Wang, S.; Moldoveanu, S. C. *J Anal Methods Chem* **2021**, *2021*, 1.

6. Olmo, F.; Garoz-Ruiz, J.; Colina, A.; Heras, A. *Anal Bioanal Chem* **2020**, *412*, 6329.

7. Wong, A.; Santos, A. M.; Fatibello-Filho, O. *Diamond Relat Mater* **2018**, *85*, 68.

8. Kamal Eddin, F. B.; Wing Fen, Y. *Sensors* **2020**, *20*, 1039.

9. Ouellette, M.; Mathault, J.; Niyonambaza, S. D.; Miled, A.; Boisselier, E. *Coatings* **2019**, *9*, 496.

10. Wu, W.-C.; Chang, H.-W.; Tsai, Y.-C. *Chem Commun* **2011**, *47*, 6458.

11. Zhang, X. *Nitric oxide (NO) electrochemical sensors, Electrochem. Sens. Biosens. Biomed. Appl*, **2008**, 1.

12. Kim, D.S.; Kang, E.-S.; Baek, S.; Choo, S.-S.; Chung, Y.-H.; Lee, D.; Min, J.; Kim, T.-H. *Sci. Rep.* **2018**, *8.*

13. Qing, W.; Liu, X.; Lu, H.; Liang, J.; Liu, K. *Microchimica Acta* **2007**, *160*, 227.

14. Alothman, Z. A.; Bukhari, N.; Wabaidur, S. M.; Haider, S. *Sens. Actuators B Chem.* **2010**, *146*, 314.

15. Zou, J.; Guan, J.-F.; Zhao, G.-Q.; Jiang, X.-Y.; Liu, Y.-P.; Yu, J.G.; Li, W.J. *J. Environ. Chem. Eng.* **2021**, *9*, 105831.

16. Chen, S.-M.; Chzo, W.-Y. *J Electroanal Chem* **2006**, *587*, 226.

17. Shang, N. G.; Papakonstantinou, P.; McMullan, M.; Chu, M.; Stamboulis, A.; Potenza, A.; Dhesi, S. S.; Marchetto, H. *Adv Funct Mater* **2008**, *18*, 3506.

Chapter 4. Summary and Conclusions

The electro-polymerization of Au NPs/Poly-terthiophene thin-film at a micro liquid|liquid interface has been studied in chapter 2. In this project, $KAuCl_4$ served as supporting electrolyte and analyte in the aqueous phase, while terthiophene was employed as monomer and electron donor in the organic phase. Three different pH of the aqueous phase were studied to investigate the effect on the morphology of electrodeposited Au NPs and the conductivity of thin-film.

By applying potential in an acceptable range, $AuCl_4^-$ was reduced to electrodeposited self-assembled Au NPs at the ITIES and TT molecules oxidized and formed cation radical of $TT^{2+\cdot}$. These $TT^{2+\cdot}$ coupled together through π-π conjugation and developed a thin-film at the ITIES. In this study, IT and ET through the ITIES were investigated in different experimental factors such as concentration ratio of $[KAuCl_4]:[TT]$, pH and applied potential. Based on the results, CVs of the blank organic phase showed $AuCl_4^-/$ $AuCl_{(4-\Upsilon)}(OH)_\gamma^-$ simple IT in negative scanning wave, however, by adding TT to the organic phase, the $AuCl_4^-/AuCl_{(4-\gamma)}\left(OH\right)_\gamma^-$ transfer wave decreased in current intensity and replaced by an ET positive peak-shaped curve.

Interfacial ET peak also increased by increasing the TT concentration in the organic phase. The other issue is that in pH 5.5 and 8.5, CVs of blank organic samples showed two simple IT peak shape waves belong to $AuCl_4^-$ and $AuCl_{(4-\gamma)}\left(OH\right)_\gamma^-$, while adding 10 mM

of HCl to the aqueous phase led to the disappearance of $AuCl_{(4-\gamma)}(OH)_{\gamma}^{-}$ transfer wave. It is assumed that the disappearance is due to the acid stabilization of $AuCl_4^-$. Then by employing SEM and TEM, the formation and morphology of the thin-film were investigated. SEM results confirmed the film formation across the ITIES, and the EDX confirmed the presence of Au NPs. According to the TEM, the morphology and structure of the Au NPs changed by varying pH, in which, at pH 5.5 and 8.5 Au NPs were cubic shape while at pH 2 it changed to star-like. Moreover, by decreasing pH, the size of Au NPs steadily increased.

In Chapter 3, an electrochemical sensor was conducted to sense DA and ascorbic acid by surface modification of carbon fiber UME. This is done by film electrogeneration with $C_{10}C_{10}$BisDTF monomer followed by Au NPs electrodeposition. Again, the film formation and electrodeposition of Au NPs on solid|solution interface at UME surface were confirmed through SEM. Based on the results, unmodified UME showed weak sensitivity regarding DA and ascorbic acid, while its' sensitivity increased by surface modification. The sensitivity of the modified UME regarding DA was higher than that of ascorbic acid. The next experiment was surface modification of UME with different concentration of $KAuCl_4$ and its effect on the detection of ascorbic acid, which showed a linear regression in calibration curve of current signal vs. ascorbic acid concentration.

4.1. Future Work

Here, different thin-films have fabricated by changing the applied potential, monomer, concentration ratio of [$KAuCl_4$]: [TT], and pH. But there is still a lot of works that can be done. The first could be manipulation of some experimental factors such as temperature, scan rate, and the number of scans to see the effect on film's conductivity and morphology of the electrodeposited Au NPs. Another try could be synthesizing of PT thin-film with other salts instead of $KAuCl_4$. Due to electrocatalytic properties of Au NPs, Au containing salts have attracted a lot of attention in the last decades; however, it is also precious to study salts containing other metal NPs like Ag, Cu, and Cd and. Ionic liquids have unique characteristics and are popular compounds for electrochemical study. During this project, DCE has been used as the organic solvent, but one possible work is using different ILs as the organic solvent. As, electrocatalytic activity of $P_{8888}TB$ has been confirmed, using that as organic solvent could be a suitable start.

Unfortunately, due to $C_{10}C_{10}$BisDTF monomer supply limitation, the UME surface modification could not be continued, and the rest of the experiments were postponed until more monomer supply. The study can be continued with a different concentration ratio of $C_{10}C_{10}$BisDTF monomer and $KAuCl_4$ to find the optimum for detection of DA. Ascorbic acid and uric acid are biological matrix that interfere the electrochemical detection of DA. Hence, electrochemical DA detection in the presence of ascorbic acid and uric acid by modified UME is another line of inquiry that can be done. Finally, changing experimental

factors like pH and temperature of the aqueous phase also can be manipulated to see the effect.

Appendix A: Co-electro-polymerization/generation of poly-terthiophene/Au nanoparticle incorporated thin-film at a micro liquid-liquid interface

Table of Contents

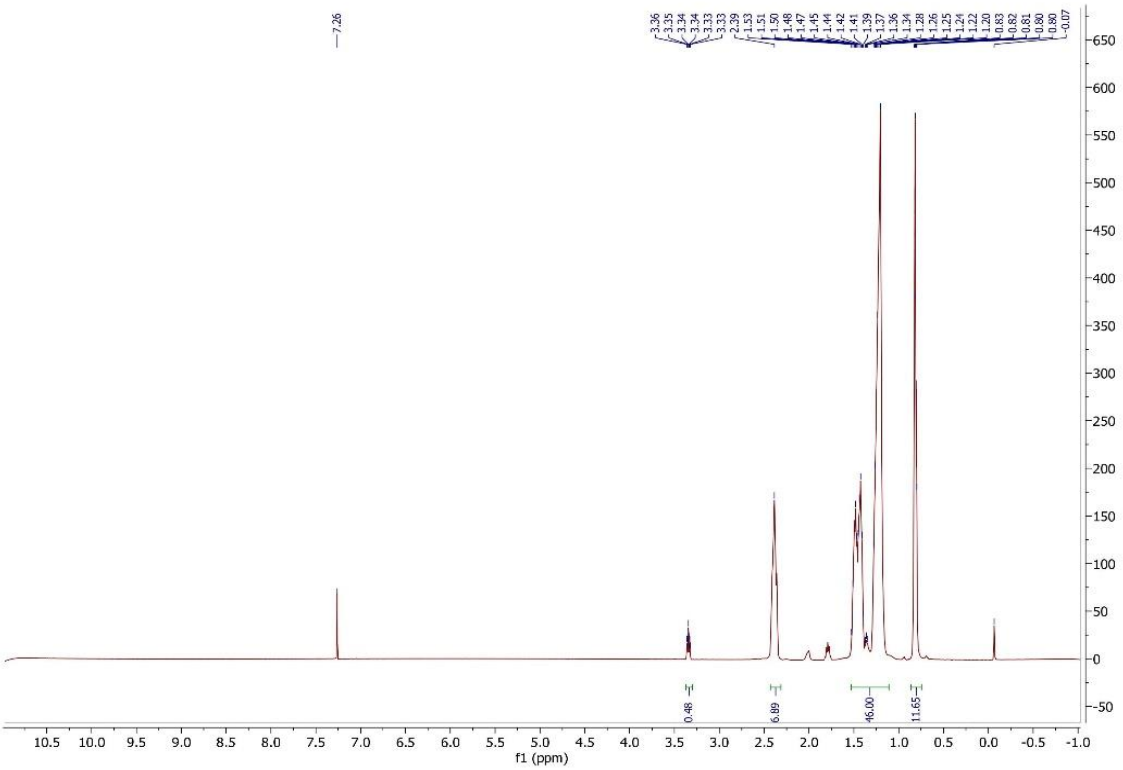

Figure A. 1 ^{1}H- NMR spectrum of $P_{8888}Br$

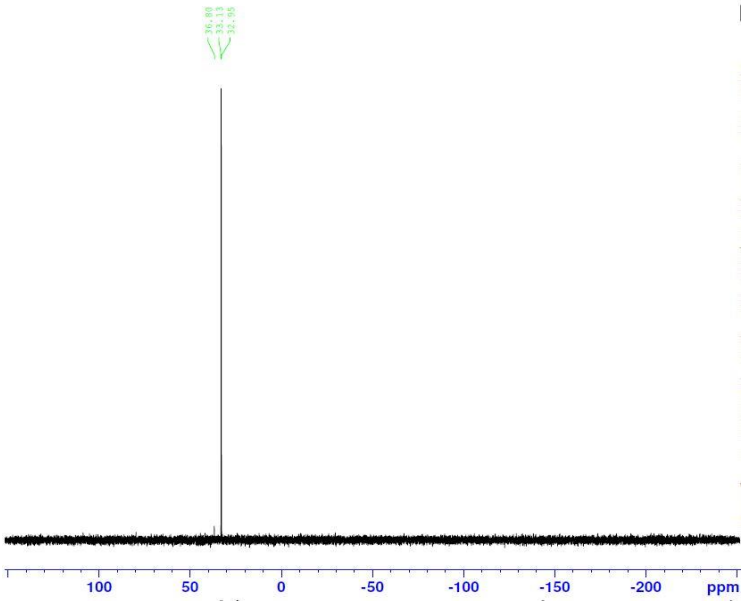

Figure A. 2 ^{31}P-NMR spectrum of $P_{8888}TB$

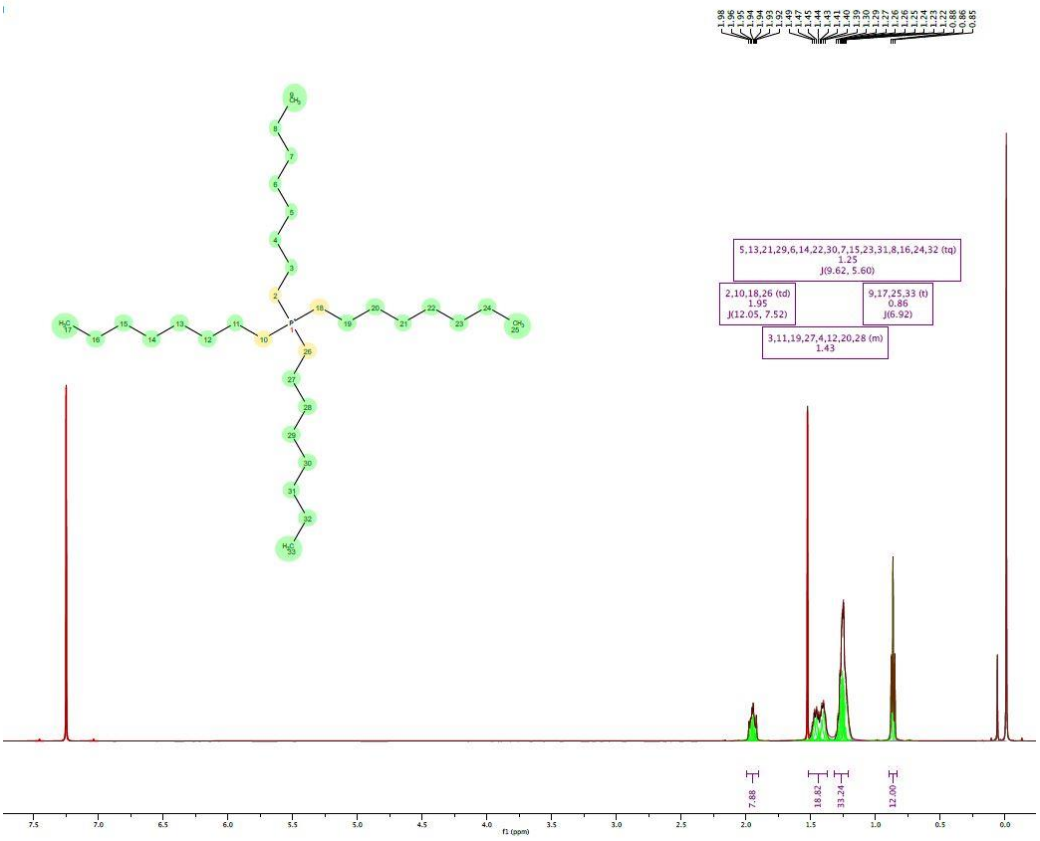

Figure A. 3 ^{1}H-NMR spectrum of $P_{8888}TB$